

# Advances in MoS<sub>2</sub>-Based Field Effect Transistors (FETs)

Xin Tong · Eric Ashalley · Feng Lin · Handong Li · Zhiming M. Wang

Received: 3 November 2014 / Accepted: 21 January 2015 / Published online: 13 February 2015  
© The Author(s) 2015. This article is published with open access at Springerlink.com

**Abstract** This paper reviews the original achievements and advances regarding the field effect transistor (FET) fabricated from one of the most studied transition metal dichalcogenides: two-dimensional MoS<sub>2</sub>. Not like graphene, which is highlighted by a gapless Dirac cone band structure, Monolayer MoS<sub>2</sub> is featured with a 1.9 eV gapped direct energy band thus facilitates convenient electronic and/or optoelectronic modulation of its physical properties in FET structure. Indeed, many MoS<sub>2</sub> devices based on FET architecture such as phototransistors, memory devices, and sensors have been studied and extraordinary properties such as excellent mobility, ON/OFF ratio, and sensitivity of these devices have been exhibited. However, further developments in FET device applications depend a lot on if novel physics would be involved in them. In this review, an overview on advances and developments in the MoS<sub>2</sub>-based FETs are presented. Engineering of MoS<sub>2</sub>-based FETs will be discussed in details for understanding contact physics, formation of gate dielectric, and doping strategies. Also reported are demonstrations of device behaviors such as low-frequency noise and photoresponse in MoS<sub>2</sub>-based FETs, which is crucial for developing electronic and optoelectronic devices.

**Keywords** MoS<sub>2</sub> FETs engineering · Low-frequency noise · Optical properties · MoS<sub>2</sub> sensors · MoS<sub>2</sub> memory devices

## 1 Introduction

TMDCs (MoSe<sub>2</sub>, MoTe<sub>2</sub>, WS<sub>2</sub>, and WSe<sub>2</sub>, etc.) are well studied layered materials with sizable bandgap, which can be changed from bulk to layered form (indirect to direct transition), thus resulting in unique physical properties that are expected to be employed in future semiconducting devices [1, 2]. In particular, molybdenum disulfide (MoS<sub>2</sub>), which is conventionally prepared by scotch tape technique and chemical vapor deposition (CVD) method, has been a

subject of great interest for several decades due to its interesting electronic and optical properties in its layered form, nanostructure and other architectures [3–12]. Numerous studies worldwide have studied how to apply this promising material in next-generation electronic and optoelectronic devices such as resonators [13], phototransistors [14], chemical sensors [15], photodetectors [16], amplifiers [17], and batteries [18, 19]. Specially, controllable valley polarization of MoS<sub>2</sub> layered material suggests its potential in valleytronic devices [20, 21]. Being an example of the simplest form of layered MoS<sub>2</sub>, monolayer MoS<sub>2</sub> has been under intensive investigation, in contrast to graphene [22], another monolayer of carbon, which remains immature due to its gapless characteristic. Several research groups have also investigated nanostructures of MoS<sub>2</sub> in fabricating MoS<sub>2</sub> devices, including nanosheet and nanoribbon transistors [23–25]. Bandgap of MoS<sub>2</sub> layered structure varies from 1.2 eV for indirect bandgap to 1.9 eV for direct bandgap [26], playing a critical role in the development of future semiconductor devices, esp.

---

X. Tong · E. Ashalley · F. Lin · Z. M. Wang (✉)  
Institute of Fundamental and Frontier Sciences, University of  
Electronic Science and Technology of China, Chengdu 610054,  
People's Republic of China  
e-mail: zhmwang@gmail.com

H. Li · Z. M. Wang  
State Key Laboratory of Electronic Thin Films and Integrated  
Devices, University of Electronic Science and Technology of  
China, Chengdu 610054, People's Republic of China

optoelectronic devices. Since the first investigation of single-layer MoS<sub>2</sub>-based transistor and MoS<sub>2</sub>-based FET structure has become an important issue in electronic and optoelectronic devices evolution, additional knowledge in this respect is necessary for enhancing the performance of MoS<sub>2</sub>-based FET in future electronic and optoelectronic devices.

## 2 MoS<sub>2</sub>-Based FETs Engineering

### 2.1 Contact Engineering

MoS<sub>2</sub>-based FET has been demonstrated to exhibit high ON/OFF ratio exceeding 10<sup>8</sup>, suggested hundreds of mobilities and low subthreshold swing at room temperature, indicating its potential employment in future electronic devices [27, 28]. However, due to the obstacle of contact resistance in achieving high-performance circuit [29], it is essential to study the contact engineering as well as intrinsic properties of MoS<sub>2</sub>-based FET to approach roadmap of prospective applications of MoS<sub>2</sub> and other 2D TMDCs.

Choosing various contact metals with different work function is critical in fabricating MoS<sub>2</sub>-based FETs, low contact resistance is expected and able to form lower Schottky barrier at MoS<sub>2</sub>-metal interface, thus allowing high performance in MoS<sub>2</sub>-based FET [30, 31]. Utilizing low work function metal scandium (Sc) as contact metal have realized a low contact resistance and high carrier injection n-type MoS<sub>2</sub>-based FET, which is demonstrated to largely eliminate the effect of contact resistance, thus reaching relatively high mobility up to 700 cm<sup>2</sup> (V s)<sup>-1</sup> in a high-*k* dielectric environment (will be discussed later) [32].

Kaustav Banerjee et al. have proposed a comprehensive study of contact metals (In, Ti, and Mo) of MoS<sub>2</sub>-based FETs. Generally, carrier injection is suppressed due to the formation of tunnel barrier by 2D MoS<sub>2</sub> at the MoS<sub>2</sub>-metal interface. Meanwhile, to date, no appropriate contact metal can form ohmic contact with MoS<sub>2</sub>, resulting in the formation of Schottky barrier at MoS<sub>2</sub>-metal interface. To reduce both the Schottky barrier and contact resistance of MoS<sub>2</sub> FET, metal In performs well to some degree but creates a large tunnel barrier; in contrast, tunnel barrier is barely observed when using Pd as the contact metal to MoS<sub>2</sub> [33]. Furthermore, employing metal Ti as contact metal can lead to a lower Schottky Barrier. However, it is still able to reduce the injection of electrons and the unstable properties of Ti also limit its high performance in MoS<sub>2</sub> FETs [34].

To overcome the difficulties mentioned above, Kaustav Banerjee et al. propose an effective method to utilize Mo as contact metal and fabricate Mo (10 nm)/Au (100 nm)

source/drain contacts on the Al<sub>2</sub>O<sub>3</sub>/Si substrate to achieve 1-layer and 4-layers MoS<sub>2</sub> FETs [35]. As illustrated in Fig. 1, the drain-source current ( $I_{ds}$ ) versus back-gate voltage ( $V_{bg}$ ) curves (blue for log scale, black for linear) for 1-layer and 4-layers MoS<sub>2</sub> FETs are shown in Fig. 1a, exhibiting evident n-type property with ON/OFF ratio exceeding 10<sup>3</sup> (under condition of 0.1 V drain-source voltage ( $V_{ds}$ )). Figure 1b describes the  $V_{bg}$  (ranging from -40 to 30 V) and corresponding contact resistance ( $R_{contact}$ ), channel resistance ( $R_{channel}$ ), and total resistance ( $R_{total}$ ) of 4-layers MoS<sub>2</sub> FET under the condition of  $I_{ds} = 0.1 \mu A$ . Compared with the contact resistance of Ti contact [36] ( $\sim 80 \text{ k}\Omega \mu m$ ) and Ni/Au contact [31] ( $\sim 4.5 \text{ k}\Omega \mu m$ ) MoS<sub>2</sub> FET, the contact resistance of Mo contact MoS<sub>2</sub> FET is much lower ( $\sim 2 \text{ k}\Omega \mu m$ ), manifesting more potential for high-performance digital circuit. In addition, Fig. 1c, d illustrates the output characteristics ( $I_{ds}$  vs.  $V_{ds}$ ) of 1-layer and 4-layers MoS<sub>2</sub> FETs with an inconspicuous Schottky contact, the black arrow denotes the increasing  $V_{bg}$  (from -30 to 30 V). Moreover, pinch-off saturation is not available for these MoS<sub>2</sub> FETs, but velocity saturation is suitable for use of as-fabricated device, which is suggested by  $\Delta I$  in Fig. 1c, d. To summarize, Mo contact multilayer MoS<sub>2</sub> FETs possess low contact resistances ( $\sim 2 \text{ k}\Omega \mu m$ ), high ON-currents (271  $\mu A \mu m^{-1}$  at  $V_{ds} = 8 \text{ V}$ ), and reasonable mobilities ( $\sim 27 \text{ cm}^2 (\text{V s})^{-1}$ ), exhibiting more potential applications in high performance digital devices than monolayer MoS<sub>2</sub> FETs.

For most of the contact metals, Fermi level pinning close to the conduction band of MoS<sub>2</sub> leads to limitation of hole injection, further detrimentally impact the realization of high-performance p-type MoS<sub>2</sub> FET. Marcio Fontana et al. have demonstrated that Pd contact metal was available to form p-type MoS<sub>2</sub> three-contact devices [37]. However, it depends a lot on large gate fields of these devices, which facilitates the decrease of Schottky barrier height in external electric field. Herein, Steven Chuang et al. introduced MoO<sub>x</sub> ( $x \leq 3$ ) as contact metal fabricated on MoS<sub>2</sub> FET, which exhibits p-type behavior, demonstrating that the MoO<sub>x</sub> is an efficient hole injection layer to MoS<sub>2</sub> [38]. As a high work function material (6.6 eV) [39], MoO<sub>x</sub> is regarded as a promising candidate for hole injector of MoS<sub>2</sub>. In this experiment, Steven Chuang et al. fabricated 30 nm Pd/30 nm MoO<sub>x</sub> contact on 260 nm SiO<sub>2</sub>/Si substrate and successfully achieve p-type MoS<sub>2</sub> FET. The schematic architecture and optical image of as-fabricated FET are shown in Fig. 2a. Figure 2b exhibits  $I_{ds}$  versus gate-source voltages ( $V_{gs}$ ) characteristics, different drain voltages ( $V_d$ ) in red curve (-0.4 V) and blue curve (-1.5 V) are measured, and locus of circle and solid line denotes experimental and simulated results, respectively. Figure 2c shows  $I_{ds}$  versus  $V_{ds}$  characteristics and  $V_{gs}$  along the arrow varying from 0 to 15 V with a 2.5 V step are

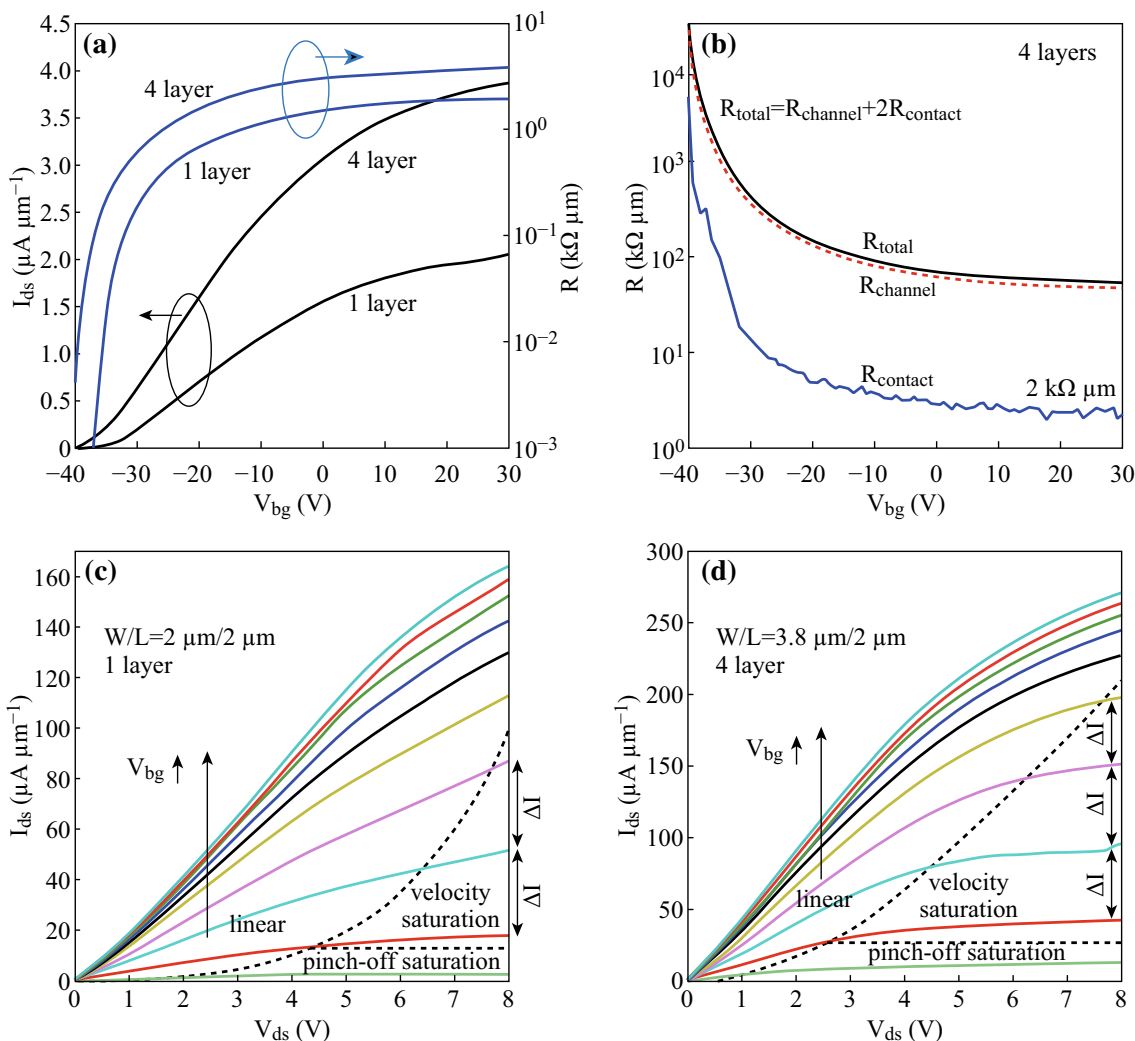


**Fig. 1** **a**  $I_{ds}$  (drain-source current) versus  $V_{bg}$  (back-gate voltage) curves for 1-layer and 4-layers MoS<sub>2</sub> FETs ( $V_{ds} = 0.1 \text{ V}$ ). **b** Different  $V_{bg}$  and corresponding contact resistance ( $R_{contact}$ ), channel resistance ( $R_{channel}$ ) and total resistance ( $R_{total}$ ) of 4-layers MoS<sub>2</sub> FET under the condition of  $I_{ds} = 0.1 \mu\text{A}$ . **c** and **d** illustrated the output characteristics ( $I_{ds}$  vs.  $V_{ds}$ ) of 1-layer and 4-layers MoS<sub>2</sub> FET, respectively. Adopted from [34]

concerned. Figure 2d displays the band diagram of as-fabricated p-type FET for the ON/OFF state. The MoS<sub>2</sub> FET with MoO<sub>x</sub> contact is demonstrated presenting evident p-type characteristics with on-current ( $I_{on}$ )/off-current ( $I_{off}$ )  $\sim 10^4$ , manifesting expected hole contact of MoO<sub>x</sub> electrode to the valence band. More importantly, this work leads to the exploration in high work function materials employed as alternative metal contacts to realize high-performance MoS<sub>2</sub>-based FETs.

At the same time, MoS<sub>2</sub>-based FETs are also supposed to be employed into applications of spintronics, which are usually fabricated by ferromagnetic contacts, thus forming the MoS<sub>2</sub>/ferromagnetic interface. Again, Schottky barrier is demonstrated to exist at this interface [40], hindering the spin injection of electrons. To reduce the Schottky barrier and investigate future spin transport of MoS<sub>2</sub>-based

devices, thin MgO layer, an additional tunnel barrier is utilized in single-layer MoS<sub>2</sub> FET (Co contact), which results in the large decrease (about 84 %) of Schottky barrier [41]. Based on this investigation, Saroj Prasad Dash et al. further introduce TiO<sub>2</sub> tunnel barrier in multilayer MoS<sub>2</sub> FET (Co contact) to tune the contact resistance, which performs well and leads to a large increase of on-state current and mobility. Moreover, the channel conductance and magnetoresistance can be controlled by applying different gate voltages, which increase the possibilities for employment of MoS<sub>2</sub> and other TMDCs for prospective applications of spintronics [42].

To study the intrinsic properties and estimate the quality of contact metals in MoS<sub>2</sub>-based FETs, four-terminal measurement is more important compared with two-terminal measurement [43, 44]. Toward this effort, N.

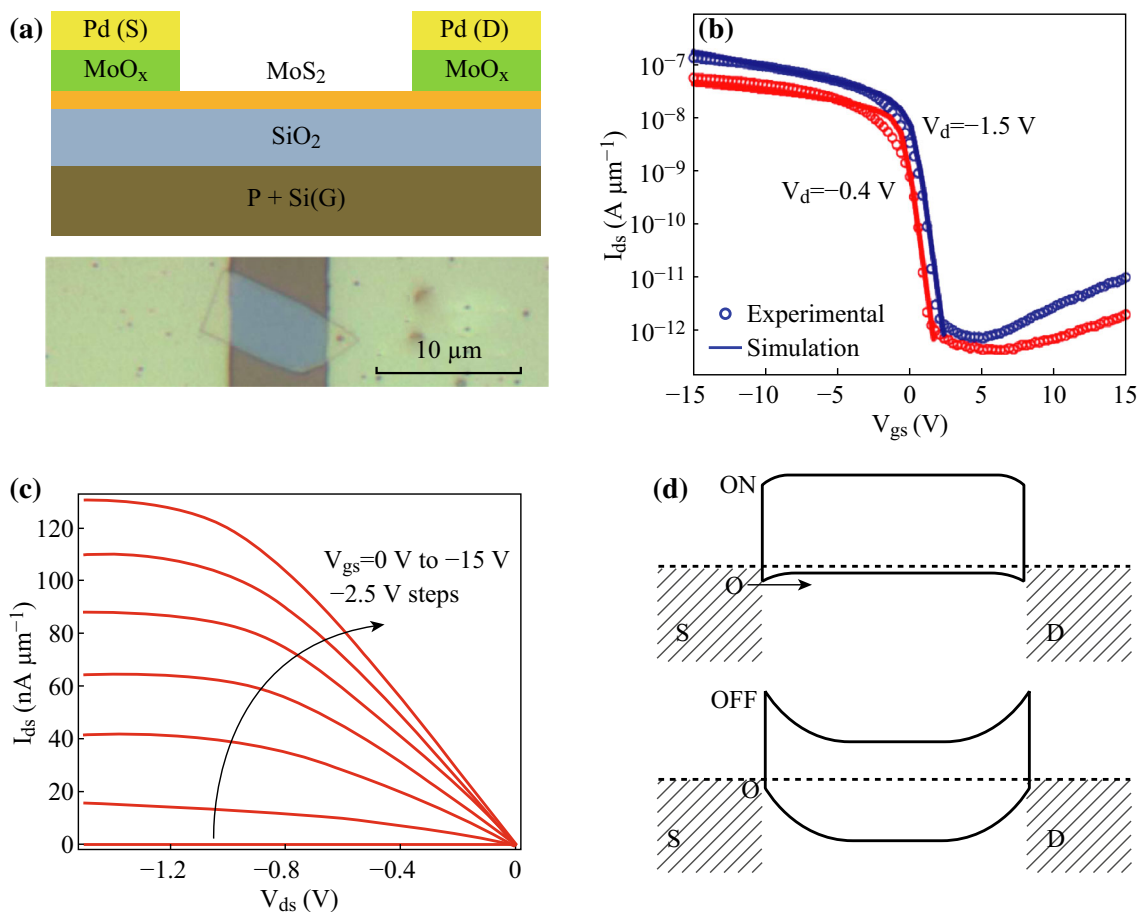


**Fig. 2** **a** Schematic architecture and optical image of as-fabricated FET. **b**  $I_{ds}$  versus  $V_{gs}$  characteristics,  $V_d$  in red curve ( $-0.4$  V) and blue curve ( $-1.5$  V) are measured, locus of circle and solid line denote experimental and simulated results, respectively. **c**  $I_{ds}$  versus  $V_{ds}$  characteristics and  $V_{gs}$  ranging from 0 to 15 V with a 2.5 V step are concerned. **d** Band diagram of as-fabricated p-type FET for the ON and OFF state. Adopted from [38]. (Color figure online)

R. Pradhan et al. fabricated the MoS<sub>2</sub>-based FET with approximate 20 layers MoS<sub>2</sub>, 300 nm silicon dioxide, and 8 Au contacts, and then, four-terminal measurement was used to study the intrinsic properties of MoS<sub>2</sub>-based FET, which could measure the effective mobility regardless of the impact of contact resistance at MoS<sub>2</sub>-metal interface. Compared with the past work by Peide D. Ye et al. [31], which was almost the same condition of as-fabricated FET, they found a large increase ( $\sim 1$  order of magnitude) of as-fabricated device in mobility ( $\sim 300$  vs.  $\sim 28$  cm<sup>2</sup> (V s)<sup>-1</sup>). In addition, Pablo Jarillo-Herrero et al. demonstrated that Hall measurement was able to nearly eliminate the contact resistance as well and Luis Balicas investigated another TMDC FET, i.e., the MoSe<sub>2</sub> FET and found that the Hall mobilities ( $\sim 250$  cm<sup>2</sup> (V s)<sup>-1</sup>) was higher than previously two-terminal measurement ( $\sim 150$ – $200$  cm<sup>2</sup> (V s)<sup>-1</sup>) [45, 46]. That is, four-terminal measurement is vital in investigating intrinsic properties of MoS<sub>2</sub>-based

FETs and estimating the quality of contact metals. Future studies about MoS<sub>2</sub>-based FETs, even TMDCs devices should pay more attention to the four-terminal measurement.

In addition, Heung Cho Ko et al. utilized graphene as the electrodes for MoS<sub>2</sub>-based FET, which was also demonstrated to effectively reduce the Schottky barrier at MoS<sub>2</sub>/graphene interface [47]. It is worth mentioning that Manish Chhowalla et al. proposed a novel method to reduce the contact resistance of MoS<sub>2</sub>-based FETs, they primarily considered two phases of MoS<sub>2</sub>: metallic 1T MoS<sub>2</sub> and semiconducting 2H MoS<sub>2</sub>, later fabricated 1T MoS<sub>2</sub> for electrodes and 2H MoS<sub>2</sub> nanosheets for channel material in FET, and then, a very low contact resistance reaching 200–300 Ω μm was achieved under none gate bias, resulting in a high ON/OFF ratio exceeding 10<sup>7</sup>, subthreshold swing (95 mV/decade) and 85 μA μm<sup>-1</sup> drive currents values [48].

## 2.2 Dielectric Formation

To achieve high-performance MoS<sub>2</sub>-based FETs, the formation of high-*k* gate dielectric is important. For example, Madan Dubey et al. fabricated the MoS<sub>2</sub> FET with and without a high-*k* Al<sub>2</sub>O<sub>3</sub> dielectric, and then, measurements of mobilities indicated an increase of 6.0–16.1 cm<sup>2</sup> (V s)<sup>-1</sup> [49]. In studies of Saptarshi Das et al. which was discussed above, they similarly introduced the high-*k* Al<sub>2</sub>O<sub>3</sub> dielectric, thus resulting in the increase of mobilities from 184 to 700 cm<sup>2</sup> (V s)<sup>-1</sup> [32]. Moreover, both theoretical and experimental studies show that high-*k* HfO<sub>2</sub> dielectric is able to effectively enhance the performance of MoS<sub>2</sub>-based FETs [27, 50, 51]. High-*k* gate dielectric is suggested to reduce the Coulombic scattering, which improves the electronic properties of channel in MoS<sub>2</sub>-based FETs [52].

Generally, considering the uniformity and controllable thickness of the material to deposit, atomic layer deposition (ALD) technology is an effective method to deposit high-*k* gate dielectric. However, high-quality gate dielectric is difficult to deposit on 2D MoS<sub>2</sub> by ALD, which attributes to the absence of dangling bonds and other active elements at the surface. Toward this effort, Peide D. Ye et al. investigated the deposition of high-*k* Al<sub>2</sub>O<sub>3</sub> on MoS<sub>2</sub> by ALD; they utilized water and trimethylaluminum (TMA) as precursor and lowered the temperature of substrate down to 200 °C, which successfully resulted in the formation of 10 nm uniform Al<sub>2</sub>O<sub>3</sub> dielectric on MoS<sub>2</sub> by physical adsorption [53]. However, reaction of precursors in low temperature could further lead to the impurities resided in as-deposited high-*k* film, which limited its electronic properties [54]. To overcome it, Hyounsub Kim et al. introduced oxygen plasma treatment in deposition of Al<sub>2</sub>O<sub>3</sub> and HfO<sub>2</sub> on multilayer MoS<sub>2</sub> by the same method of ALD; they used X-ray photoelectron spectroscopy (XPS) analysis and found that oxygen plasma-treated MoS<sub>2</sub> formed Mo-oxide layer at its surface, which is demonstrated to improve the quality of as-grown high-*k* Al<sub>2</sub>O<sub>3</sub> and HfO<sub>2</sub> dielectric. This work indicates the promising of plasma-treated ALD method in formation of high-*k* gate dielectric on MoS<sub>2</sub>-based FET [55].

Deposition of high-*k* Al<sub>2</sub>O<sub>3</sub> on ultraviolet-ozone (UV-O<sub>3</sub>)-treated MoS<sub>2</sub> has also been studied. Uniform high-*k* Al<sub>2</sub>O<sub>3</sub> film was achieved due to the removal of contaminations and the formation of slight S–O bonds at the MoS<sub>2</sub> surface. It is necessary to mention that UV-O<sub>3</sub> exposure did not break the Mo–S bonds and was a non-disruptive method to achieve high-quality Al<sub>2</sub>O<sub>3</sub> dielectric deposition. The surface of UV-O<sub>3</sub>-treated MoS<sub>2</sub> is also demonstrated to be a suitable layer for controllable deposition of uniform and ultrathin Al<sub>2</sub>O<sub>3</sub> (~4 nm), which is more practical in MoS<sub>2</sub>-based FET technology [56]. In addition, Lanxia Cheng et al. investigated the ALD deposition of Al<sub>2</sub>O<sub>3</sub> dielectric on MoS<sub>2</sub> by precursors of TMA/H<sub>2</sub>O and TMA/O<sub>3</sub> and studied

the properties of two types of as-deposited thin films. They claimed that O<sub>3</sub> was an important factor in high-quality ALD deposition, which resulted in the deposition of uniform, lower thickness (~5 nm) of dielectric layer without the S–O bonds generation at MoS<sub>2</sub> surface and the improvement of growth rate [57].

The formation of high-*k* dielectric is critical for MoS<sub>2</sub>-based FETs technology, and the nature of no dangling bonds at the surface of 2D MoS<sub>2</sub> allows discovering suitable precursors and pretreatments for ALD deposition, which is relatively effective in gate dielectric deposition. Lowering the temperature of substrate to achieve physical adsorption can lead to uniform high-*k* dielectric layer deposition, but it is limited by essential clean surface of MoS<sub>2</sub> and hard to control the parameters of deposition. Oxygen plasma-treated MoS<sub>2</sub> surface is also demonstrated to form high quality, uniform dielectric layer, but this method is regarded as destructive. These two methods are not very practical in MoS<sub>2</sub>-based FETs as the formation of uniform layer can be achieved only when the thickness is enough (about 10 nm), which limit the scaling down of FET. In contrast, UV-O<sub>3</sub> exposure and O<sub>3</sub> precursor are non-destructive and able to deposit ultrathin dielectric layer (~5 nm), which are expected in gate dielectric formation of MoS<sub>2</sub>-based FETs and other TMDCs-based FETs.

## 2.3 Doping Strategies

Appropriate doping is another effective method to achieve high-performance MoS<sub>2</sub>-based FETs, which is demonstrated to strongly affect the contact resistance of MoS<sub>2</sub> FET instead of utilizing different contact metals, such as n-type doping from polyethyleneimine (PEI) molecules on multilayer MoS<sub>2</sub>-based FET [58]. Ultrathin MoS<sub>2</sub> limits the doping methods (ion implantation, etc.) employed in other semiconductors, leading to the exploration of novel doping methods in MoS<sub>2</sub>-based FET technology.

Cesium Carbonate (Cs<sub>2</sub>CO<sub>3</sub>) has been employed to dope monolayer MoS<sub>2</sub> FET [59], resulting in stable n-type doping and largely enhance the electron concentration in monolayer MoS<sub>2</sub> (about 1 order of magnitude). Potassium has also been demonstrated to achieve degenerate n-doping of MoS<sub>2</sub> FET in vacuum, indicating the essential of degenerate doping in high-performance MoS<sub>2</sub> FET [60]. However, the unstable nature of Potassium limits its practical application. Herein, Daisuke Kiriya et al. proposed a doping strategy based on benzyl viologen (BV) [61], as illustrated in Fig. 3. Figure 3a depicts the schematic diagram of BV doping on trilayer MoS<sub>2</sub> FET and the as-fabricated FET was put into the BV solution for 12-h doping; transfer characteristics of as-fabricated MoS<sub>2</sub>-based FET with and without doping are compared and shown in Fig. 3b. Before BV doping, the ON/OFF of MoS<sub>2</sub> FET mainly depends on V<sub>gs</sub> (ranging from –40 to

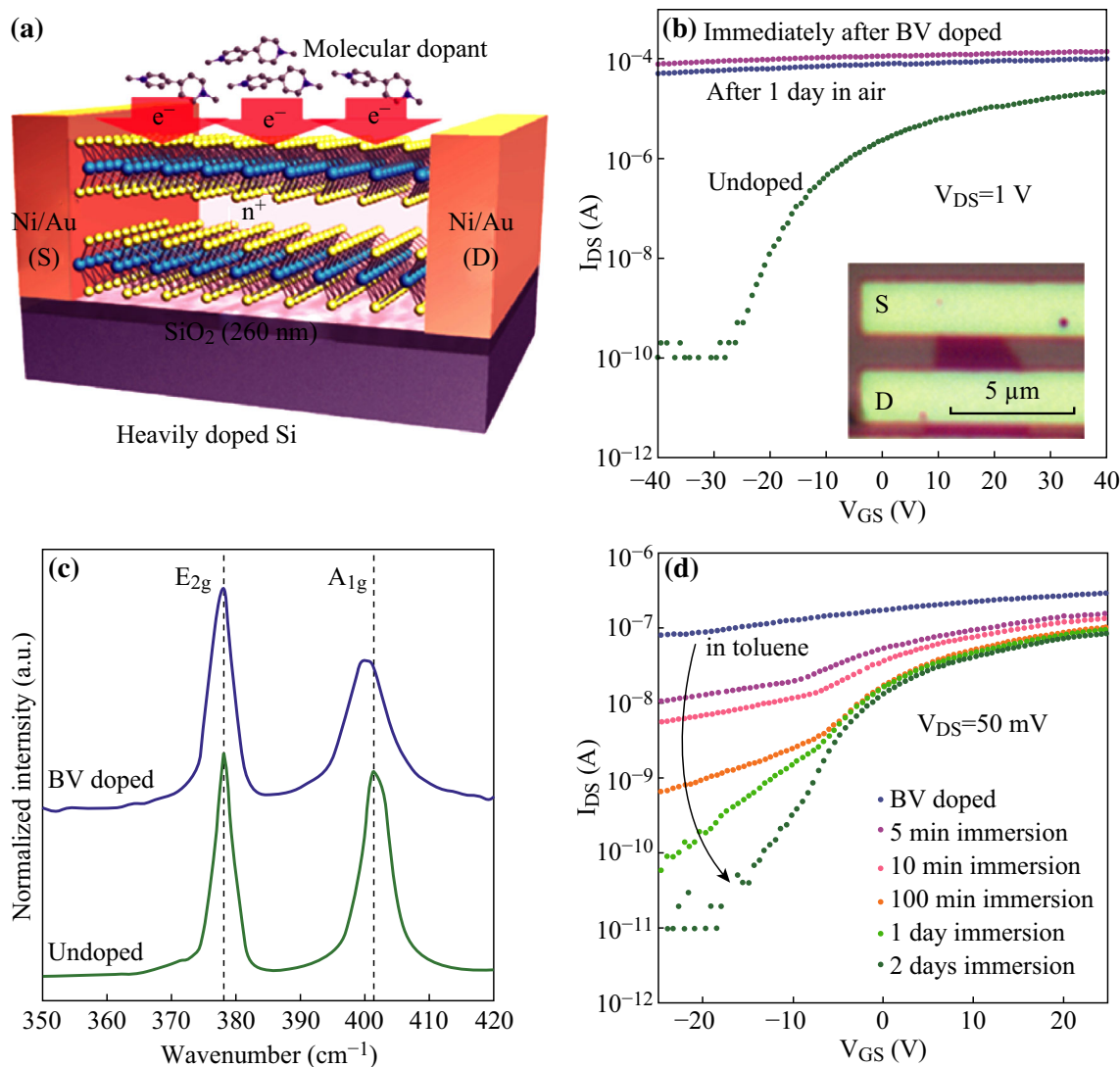


**Fig. 3** **a** Schematic diagram of BV doping on trilayer MoS<sub>2</sub> FET. **b** Transfer characteristics of as-fabricated MoS<sub>2</sub>-based FET with and without doping. **c** Raman spectroscopy measurement. **d** Transfer characteristics of as-fabricated MoS<sub>2</sub>-based FET with different time in toluene. Adopted from [61]

40 V) and the  $I_{ds}$  is about  $2 \times 10^{-5}$  A ( $V_{gs} = 40$  V), following that BV doping indicates the less dependence of  $V_{gs}$  and the increase of  $I_{ds}$ , which demonstrates the effective doping of BV method. Raman spectroscopy measurement is shown in Fig. 3c, depicting a red shift and realization of high electron density. Moreover, Fig. 3d shows that the as-doped FET is put into toluene and corresponding transfer characteristics with different time, which is promising for tuning the dopants density. This work represents an effective n-type doping method, which also reduces the contact resistance and improves the performance of MoS<sub>2</sub>-based FET.

Elements from halogen family are promising in doping MoS<sub>2</sub>. Toward this effort, chloride (Cl) molecular has been utilized to dope MoS<sub>2</sub> FET by Lingming Yang et al. [62].

Few layer MoS<sub>2</sub> is immersed into 1, 2 dichloroethane (DCE) over 12 h and then fabricated in MoS<sub>2</sub> FET; n-type doping is elucidated by change of Fermi level, which is measured by XPS at the surface before and after doping. More importantly, the contact resistance of as-fabricated FET is reduced to a very low value (0.5 kΩ μm) after Cl molecular doping, thus resulting in a high drain current (460 mA mm<sup>-1</sup>). In addition, WS<sub>2</sub> FET is also doped by the same method and even more effective than MoS<sub>2</sub> FET, indicating that the Cl molecular doping is available in other TMDCs.

Doping strategies are significant in MoS<sub>2</sub>-based FETs and other TMDCs-based devices, and proper doping methods are expected in FET fabricated from ultrathin

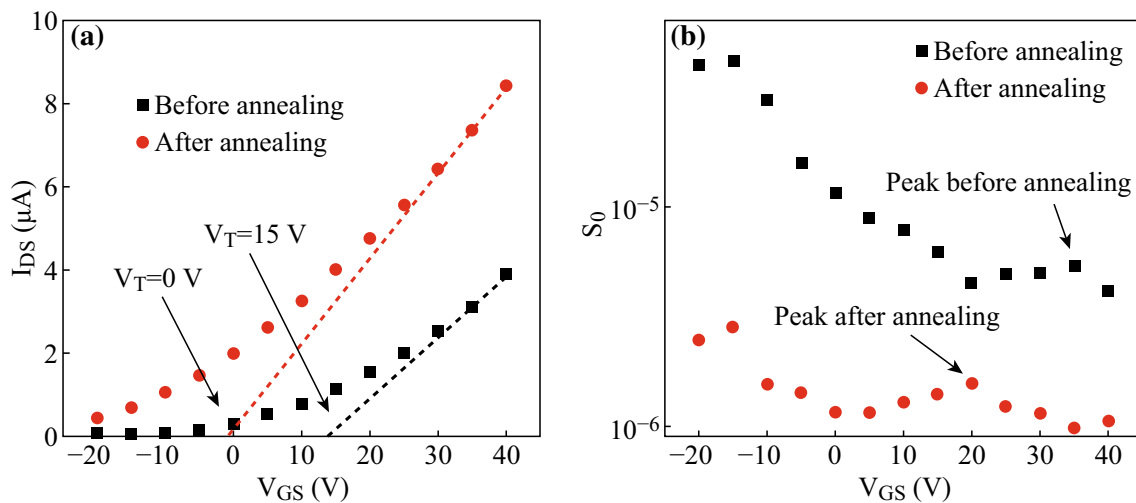


**Fig. 4** **a**  $I_{ds}$  versus  $V_{gs}$  characteristics at  $V_{ds} = 3$  V of this FET, the red locus of points represents the curve after annealing ( $V_T = 0$  V) and black locus of points represents the curve before annealing ( $V_T = 15$  V). **b** The noise measurements before and after annealing at  $V_{ds} = 3$  V. Adopted from [72]. (Color figure online)

semiconducting materials. Note that, doping methods of 2D materials are still immature; studies are essential to explore stable, effective, and controllable doping strategies, which are practical and convenient in future nanoelectronic and optoelectronic devices.

### 3 Low-Frequency Noise (LFN) Analysis in MoS<sub>2</sub>-Based FETs

The low-frequency noise (LFN) has been demonstrated as a limiting factor in high-performance electronic devices [63] and is generally called  $1/f$  noise or flicker noise, which is first discovered in 1925 [64]. LFN determines the

minimum value of signal level in electronic devices and circuits, affecting the realization of scaling down and lower power consumption in future circuits [65, 66], showing that it is necessary to study the LFN in MoS<sub>2</sub>-based FETs as this 2D layered material has been widely utilized for the fabrication of ultrascaled FET [67] and integrated circuits [68]. Analysis of LFN (measure the fluctuations of mobility conductivity or fluctuation of FET channel induced by carrier trapping or de-trapping) can help evaluate the quality of MoS<sub>2</sub> FET [69]. Furthermore, for practical usage of MoS<sub>2</sub> FET analog and digital electronic devices, it is necessary to reach the minimum requirement of LFN [70, 71].

Toward this effort, the LFN of bilayer MoS<sub>2</sub> FET has been studied in details by Xie et al. [72]. The MoS<sub>2</sub> FET is fabricated by a 1.2-nm-thick MoS<sub>2</sub> (bilayer) thin film on a 300 nm SiO<sub>2</sub>/highly doped n-type Si substrate with 30-nm Ti/100-nm Au film as electrodes. The corresponding noise characteristics are measured and a new model of understanding the LFN in bilayer MoS<sub>2</sub> FET was proposed. Different from 3D materials, the results exhibit a longer trap decay time in 2D materials with van der Waals bond (MoS<sub>2</sub>). Based on this model, an annealing is processed toward this bilayer MoS<sub>2</sub> FET. Figure 4a shows the  $I_{ds}$  versus  $V_{gs}$  characteristics ( $V_{gs}$  ranging from  $-20$  to  $40$  V) at  $V_{ds} = 3$  V of this FET, the red locus of points represents the curve after annealing under condition of no threshold voltage ( $V_T$ ), and black locus of points represents the curve before annealing ( $V_T = 15$  V), respectively. Figure 4b exhibits the noise measurements ( $V_{gs}$  ranging from  $-20$  to  $40$  V) before and after annealing at  $V_{ds} = 3$  V. A remarkable movement of noise peak to lower  $V_{gs}$  after

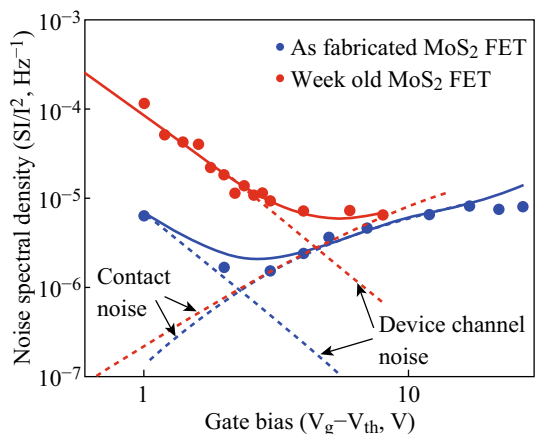


**Fig. 5** Noise spectral density as a function of gate bias before and after aging in as-fabricated MoS<sub>2</sub> device. Adopted from [75]

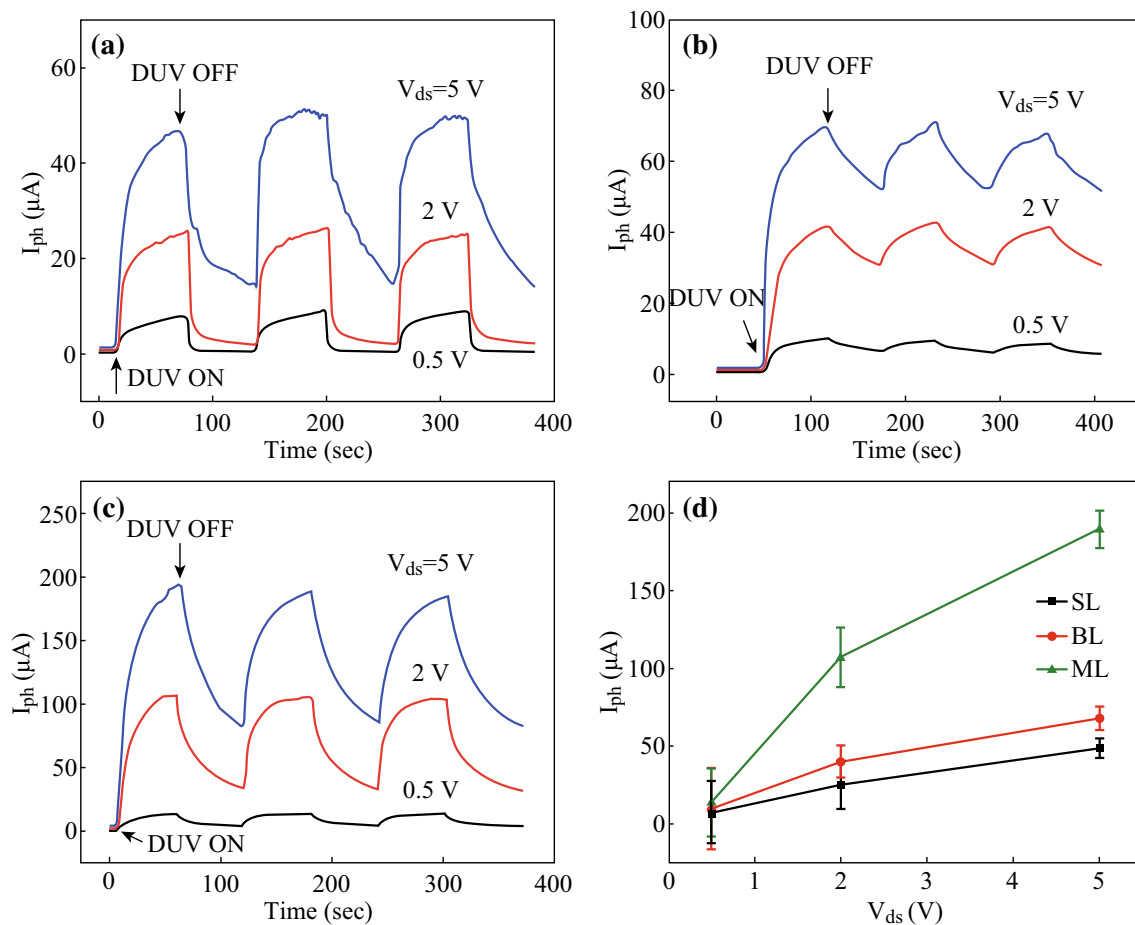


**Fig. 6** a–c Photocurrent ( $I_{ph}$ ) of monolayer, bilayer and multilayer MoS<sub>2</sub> FETs measured in air (under the condition of  $V_{ds} = 0.5, 2.0, 5.0$  V and  $V_G = 0$ ), respectively. **d** Relative  $I_{ph}$  as a function of  $V_{ds}$  (0–5 V). Adopted from [80]

annealing was observed, indicating that the decrease of trap density (annealing process) can effectively reduce the LFN in as-fabricated MoS<sub>2</sub> FET.

While  $1/f$  noise has been investigated in monolayer [73] and bilayer MoS<sub>2</sub> FET, study of LFN in multilayer MoS<sub>2</sub> FET is essential for its optimization. In order to achieve these goals, Kwon et al. [74] have investigated the LFN in multilayer MoS<sub>2</sub> FET, which is architected with a 40–50-nm MoS<sub>2</sub> thin-film channel layer, 10 nm Ti/300 nm Au contact, and SiO<sub>2</sub> on p-type silicon substrate. They studied the LFN behavior  $1/f^\gamma$  of as-fabricated MoS<sub>2</sub> FET, where the  $\gamma$  is an exponent associated with distribution of traps. With the increase of gate voltage ( $V_G$ ), the trap in as-fabricated FET will be filled and  $\gamma$  will decrease and be stable at a value of 0.95. In contrast to the dominance of mobility fluctuation noise mechanism in monolayer MoS<sub>2</sub> FET [73], the dominance of noise mechanism in as-fabricated multilayer MoS<sub>2</sub> FET is demonstrated to be the carrier number fluctuation. Moreover, they found LFN characteristics of multilayer MoS<sub>2</sub> FET are better than monolayer MoS<sub>2</sub> FET, which attributes to its lower Hooge parameter related

to the level of LFN. In addition, Renteria et al. [75] studied the relative contribution of channel and contact for LFN in multilayer MoS<sub>2</sub> FET and demonstrated that the main mechanism of LFN is carrier number fluctuation, as depicted by Kwon et al. Moreover, they proposed a comparison of as-fabricated multilayer MoS<sub>2</sub> FETs before and after aging. Figure 5 shows the noise spectral density before and after aging. It has been observed that the channel noise of MoS<sub>2</sub> FET increased more than one order of magnitude after aging, but the increase of contact noise is very few. Thus, the phenomenon is mainly caused by the aging of the MoS<sub>2</sub> channel rather than the aging of contact. This new phenomenon can be utilized in MoS<sub>2</sub>-based FET and other TMDCs-based FETs in terms of the optimization in channel implementation.

In addition, MoS<sub>2</sub>-metal contacts of MoS<sub>2</sub>-based FETs are also demonstrated to impact LFN [76]. The vacuum annealing strongly increases the transparency of contacts in FET, thus resulting the decrease of LFN. To conclude, LFN has been investigated in MoS<sub>2</sub>-based FETs, indicating the related factors are trap density, channel, and contact, which

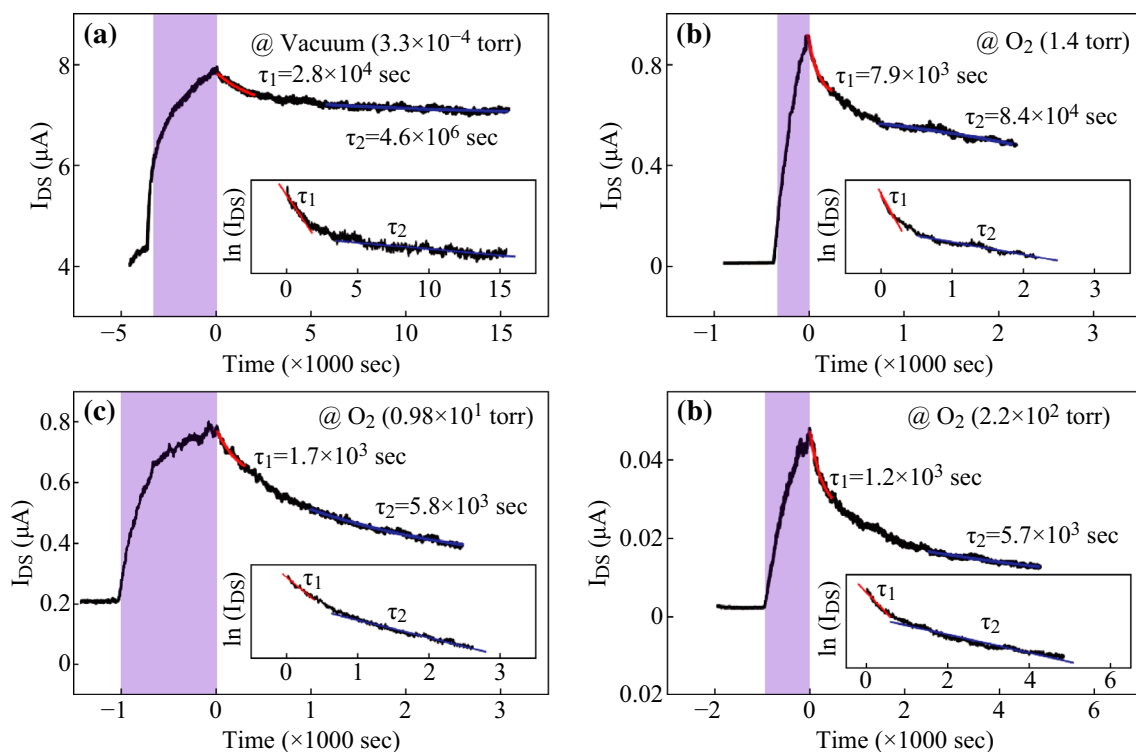


**Fig. 7** Photocurrent measurement under **a**  $3.3 \times 10^{-4}$  Torr vacuum condition, the shadow region means the UV light is on **b-d** shows the measurements under oxygen condition of 1.4 Torr,  $0.98 \times 10^1$  Torr, and  $2.2 \times 10^2$  Torr, respectively. Adopted from [81]

should be concerned for future circuits based on MoS<sub>2</sub> and other 2D TMDCs.

#### 4 Optical Properties of MoS<sub>2</sub>-Based FETs

TMDCs have been widely fabricated in P–N junction devices, heterostructures, and phototransistors due to the outstanding photovoltaic effect [2, 77, 78]. Particularly, MoS<sub>2</sub>-based FETs have already been demonstrated to show a strong photoresponse [79]. To comprehensive study the optical properties of MoS<sub>2</sub>-based FETs, the number of MoS<sub>2</sub> layers is concerned; herein, Jonghwa Eom et al. investigated layer-dependent MoS<sub>2</sub> FETs (monolayer, bilayer, and multilayer) and measured the photocurrent response under different  $V_{ds}$  by using a 220 nm deep ultraviolet (DUV) light [80]. In Fig. 6, photocurrent ( $I_{ph}$ ) of monolayer, bilayer, and multilayer MoS<sub>2</sub> FETs was measured in air (under the condition of  $V_{ds} = 0.5, 2.0, 5.0$  V and  $V_G = 0$ ) and illustrated in Fig. 6a–c, respectively. Figure 6d summarizes the results from Fig. 6a–c as a function of  $V_{ds}$  (0–5 V). They observed that monolayer and bilayer MoS<sub>2</sub> FET exhibited a smaller value of photocurrent than multilayer MoS<sub>2</sub> FET, which mainly attributed to a narrower bandgap and higher density of states in multilayer MoS<sub>2</sub> FET. After turning off the light, relaxation time of photocurrent response was also measured in monolayer,

bilayer, and multilayer MoS<sub>2</sub> FETs; again, the smaller bandgap of multilayer MoS<sub>2</sub> resulted in a shorter relaxation time in multilayer MoS<sub>2</sub> FET. This work suggested that multilayer MoS<sub>2</sub> FET was more promising than few layer MoS<sub>2</sub> FET in photovoltaic applications, and as discussed above, multilayer MoS<sub>2</sub>-based FET with graphene electrode not only reduced the Schottky barrier height at MoS<sub>2</sub>/graphene interface, but shows a 74 % optical transmittance (wavelength ranging from 400 to 800 nm), which is promising for transparent devices [47].

The photocurrent of MoS<sub>2</sub> FET is always a significant topic to discuss. Cho et al. [81] have studied the decay of photocurrent in MoS<sub>2</sub> FET; they fabricated the multilayer MoS<sub>2</sub> nanosheet FETs and measured the decrease of photocurrent before and after turning off the UV light. Figure 7 illustrates the photocurrent measurements at different atmosphere in the same  $V_{ds}$  (0.1 V), and two constant of decay time  $\tau_1$  and  $\tau_2$  are also shown in Fig. 7. Figure 7a exhibits the photocurrent measurement under  $3.3 \times 10^{-4}$  Torr vacuum condition (shadow region represents on-state UV light). Figure 7b–d exhibits the measurements under oxygen condition of 1.4 Torr,  $0.98 \times 10^1$  Torr, and  $2.2 \times 10^2$  Torr. With the increase of oxygen pressure, photocurrent decreases faster, which is attributed to the charge trapping at the associated oxygen defect sites on MoS<sub>2</sub> surface. In addition, they measured the decrease of photocurrent under different gate-bias stresses and found

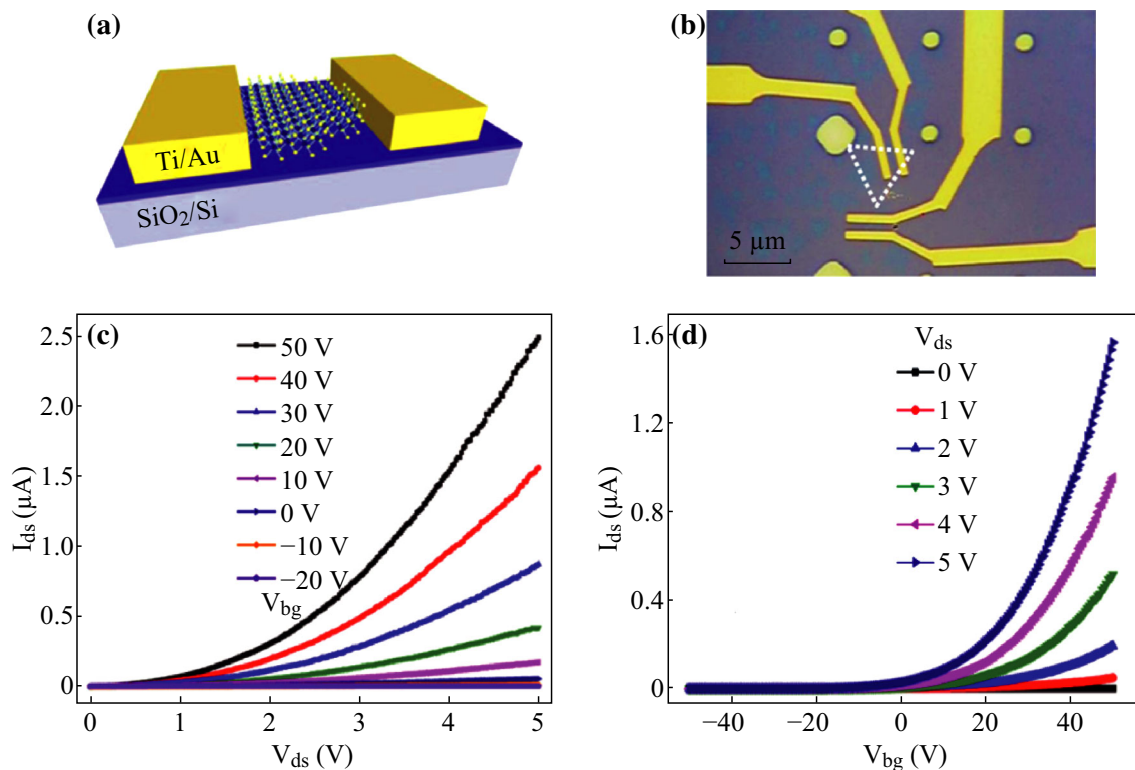


**Fig. 8** **a** Schematic diagram and **b** Optical image of the MoS<sub>2</sub> FETs. **c** Output characteristics ( $I_{ds}$  vs.  $V_{ds}$ ) and **d** Transfer characteristics ( $I_{ds}$  vs.  $V_{bg}$ ) of the MoS<sub>2</sub> FETs. Adopted from [88]

that when the gate-bias stress was negative, the decrease of photocurrent became slower and vice versa. Further study revealed that this phenomenon was caused by the increase of charge trapping (oxygen site) on MoS<sub>2</sub> interface as well [82]. Moreover, resonant plasmonic nanoshells have also been deposited to fabricate MoS<sub>2</sub> FET, which is demonstrated to be capable for the enhancement of photocurrent and photoluminescence [83].

As discussed above, regarding the transient time constant, isolated MoS<sub>2</sub> FET manifested its potential in optoelectronics, which could reach magnitude of millisecond. However, Feng Wang et al. have investigated the optical properties of MoS<sub>2</sub>-WS<sub>2</sub> heterostructure and the ultrafast dynamics of hole transfer and found a remarkable rise time shorter than 50 fs, which is demonstrated to hold large promising in future optoelectronic applications [84]. Based on this novel investigation, Su-Huai Wei et al. fabricated MoS<sub>2</sub>-WS<sub>2</sub> heterostructure-based FET, which was demonstrated to possess high ON/OFF ratio exceeding 10<sup>5</sup> and high photoresponsivity reaching 1.42 A W<sup>-1</sup> [85].

The photoresponse of MoS<sub>2</sub>-based FETs shows promising for prospective applications of optoelectronics, compared with few layer MoS<sub>2</sub>; multilayer MoS<sub>2</sub> is demonstrated to manifest better performance in photocurrent generation. Moreover, plasma-treated, novel nanostructured, and

heterostructured MoS<sub>2</sub> are expected to fabricate high-performance MoS<sub>2</sub>-based FETs.

## 5 MoS<sub>2</sub>-Based FETs Applications

### 5.1 Applications of MoS<sub>2</sub>-Based FETs in Sensors

Due to the planar, atomic thin structure, possibility of large scale preparation, high surface-to-volume ratio and

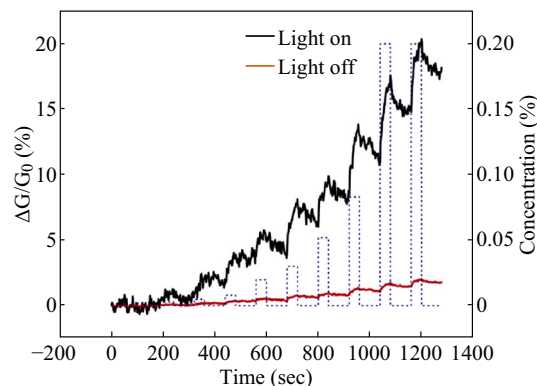


**Fig. 9** Sensitivity of triethylamine (TEA) with and without illumination. *Black line* represents on-state light and *red line* for off state. Adopted from [92]. (Color figure online)

suggested bandgap, MoS<sub>2</sub>-based FET has been studied in sensor applications. Toward this effort, high-sensitivity pH sensor with reasonable range (3–9) and selectivity biosensor for protein detection (available at 100 femtomolar concentration) have been achieved by MoS<sub>2</sub>-based FET [86]. Similarly, for label-free biosensors, MoS<sub>2</sub> nanosheet is promising and fabricated in FET, which exhibits high sensitivity in detecting cancer biomaker [87]. The as-fabricated FET is employed in liquid phase to selectively detect prostate-specific antigen (PSA) (cancer biomaker) by the change of drain current. That is, this method is potential for facilitating the development of cancer diagnostics in earlier time.

For gas sensor, Liu et al. [88] have focused on the Schottky-contacted CVD grown monolayer MoS<sub>2</sub> FET. They fabricated the MoS<sub>2</sub> FETs with 5 nm Ti/50 nm Au metal contact; the schematic diagram and optical image of MoS<sub>2</sub> FETs are shown in Fig. 8a, b, respectively. Figure 8c exhibits the  $I_{ds}$  versus  $V_{ds}$  output characteristics of as-fabricated FET, and transfer characteristics ( $I_{ds}$  vs.  $V_{bg}$ ) is illustrated in Fig. 8d, manifesting the n-type characteristic, which corresponds to the n-type electronic property of MoS<sub>2</sub> semiconductor [89]. Note that, there exists a Schottky barrier (SB) in as-fabricated MoS<sub>2</sub> FET-based sensor (Fig. 8c). Later, they investigated the sensitivity and the mechanism of as-fabricated FET for detecting two poisonous gases: NO<sub>2</sub> and NH<sub>3</sub>. Generally, conductance (resistance) change is measured to reflect performance of sensing and total resistance of as-fabricated FET is expressed as follows:

$$R = R_{\text{channel}} + R_{\text{contact}} \quad (1)$$

In this equation,  $R_{\text{channel}}$  is only related to carrier concentration, but  $R_{\text{contact}}$  is related to both carrier concentration and the Schottky barrier height. The relationship is exponential, thus indicating that the Schottky barrier is a key factor in sensitivity. With a conductance change larger than 20 and 40 %, the sensitivity of this MoS<sub>2</sub> FET-based chemical sensor can reach 20 parts per billion (ppb) for NO<sub>2</sub> and 1 parts per million (ppm) for NH<sub>3</sub>, respectively. This detection limit is the lowest gas concentration detected compared with the other experiments: Li et al. [90] used multilayer MoS<sub>2</sub> film FET to detect NO (detection limit ~800 ppb) and Late et al. [91] presented a detection limit of several hundred ppm for both NH<sub>3</sub> and NO<sub>2</sub> using atomically thin-layered MoS<sub>2</sub> transistors. Moreover, Liu et al. found part of MoS<sub>2</sub> devices exhibiting more Ohmic contact, but the little conductance change (<5 %) upon exposure to NO<sub>2</sub> at concentrations up to 400 ppb further manifests that Schottky barrier modulation plays a more important role in these MoS<sub>2</sub> FET-based sensors. That is, it is realizable to modulate the Schottky barrier contact of MoS<sub>2</sub>-based FET sensor and achieve higher performance at the sub-ppb level.

Moreover, in monolayer MoS<sub>2</sub>-based FET sensor, sensitivity of detecting triethylamine (TEA) can be enhanced by illumination [92] as illustrated in Fig. 9.  $\Delta G$  stands for the decrease of initial conductance ( $G_0$ ) of FET when exposed to TEA, the calculated  $\Delta G/G_0$  is the sensitivity. The black line represents that the light is on and red line for off state, showing the increase of sensitivity with longer time (about 1 order of magnitude), which may attributes to the enhancement of conductivity under illumination. Convenient way of fabricating MoS<sub>2</sub>-based FET sensor is expected, which is significant in practical applications [25]. In addition, Lee et al. fabricated the sensor without dielectric layer on multilayer MoS<sub>2</sub> FETs, which possess hydrophobic interface that serves as novel non-dielectric layer, thus resulting in the improvement of sensitivity [93]. With the nature of 2D structure, MoS<sub>2</sub>-based FET sensors should be studied further to explore higher sensitivity, lower cost, more effective biosensors, and chemical gas sensors, which are potential for next-generation medical diagnosis of cancer, environment monitoring, and food safety.

## 5.2 Applications of MoS<sub>2</sub>-Based FETs in Memory Devices

Multibit memory devices have attracted much attention and investigations, which are generally fabricated by organic semiconductor materials [94], nanostructure materials [95], and phase-change materials [96]. It is significant to explore a novel convenient method to fabricate multibit memory. Toward this effort, Chen et al. [97] have explored an approach to fabricated MoS<sub>2</sub> FET-based 2–4 bit memory devices. They proposed a plasma-treated way and found that this plasma-treated MoS<sub>2</sub> FET could act as multibit memory devices as illustrated in Fig. 10. Figure 10a is the schematic diagram of plasma-treated MoS<sub>2</sub> FET, of which a 15–30-nm MoS<sub>2</sub> film served as the active layer with 5 nm Ti/50 nm Au electrode. The optical image of as-treated MoS<sub>2</sub> FET is shown in Fig. 10b. Herein, D and S are the Ti electrode and Au electrode, respectively. Figure 10c shows the transport characteristic curve ( $I_{DS}$  ( $I_{ds}$ ) vs.  $V_G$ ); in addition, the measurements of retention are given in Fig. 10d, and it can be seen that the write/read ratio is about 10<sup>3</sup> after 1 h and 400 after 3 days. Accordingly, a write/read ratio value of about 64 of the as-fabricated FET aged after 10 years can be inferred, which is still valid for circuit application. It is further found that the plasma-treated MoS<sub>2</sub> FET is faster in programing than the untreated one in their experiments. A physical model for explaining the performance enhancement was proposed as following: The plasma-treated channel top layer could be separated and forms an ambipolar charge-trapping layer, allowing the high-performance non-volatile retention and multibit states

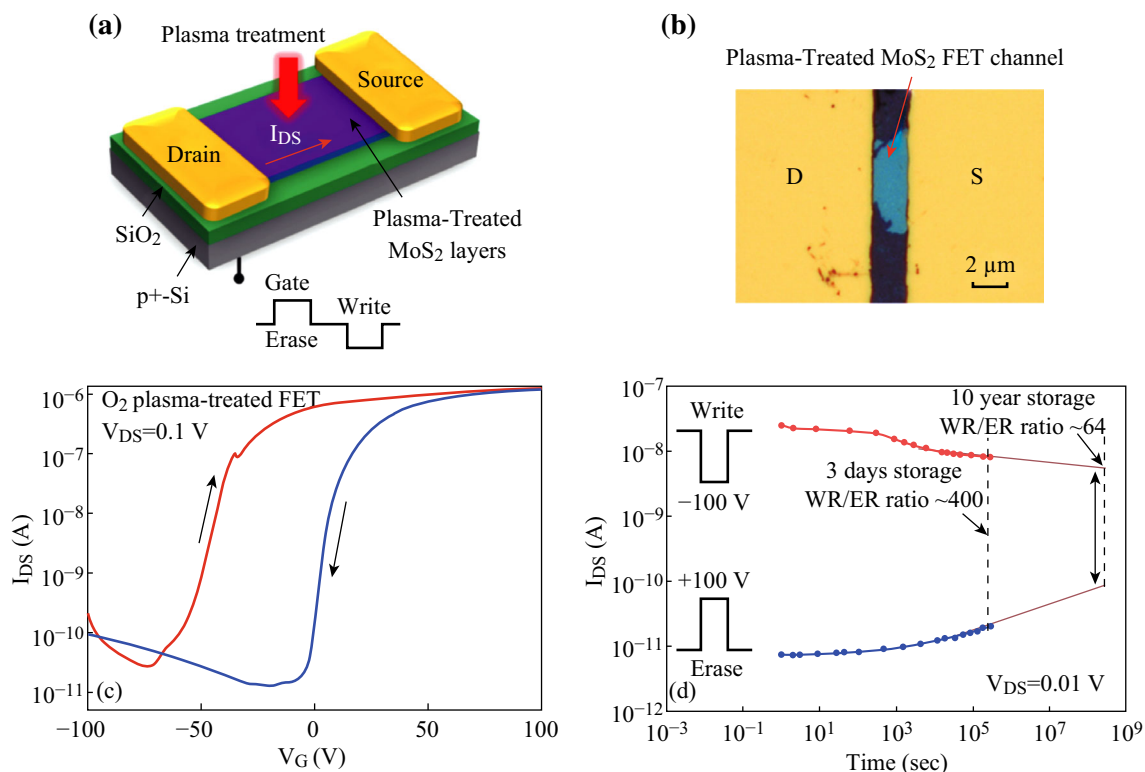


**Fig. 10** **a** The schematic diagram of plasma-treated MoS<sub>2</sub> FET. **b** The optical image of as-treated MoS<sub>2</sub> FET. **c** Transfer characteristic curve ( $I_{DS}$  vs.  $V_G$ ). **d** Retention measurements of this FET. Adopted from [97]

in this FET. This method is certainly worth considering for fabrication of nanodevices since it is technically convenient and provides a relatively simple way for realizing non-volatile memory devices, which also offers an effective method to scale down current circuit in future nanoelectronics.

Moreover, MoS<sub>2</sub> nanoflakes have been employed as charge-trapping layer (nano-floating gate) to fabricate organic nano-floating gate memories (NFGMs) by Kang et al. [98], which are based on organic (poly (3-hexylthiophene) (P3HT)) FET. The inserted solution process is convenient and realized at low temperature to introduce MoS<sub>2</sub> nanoflakes between two dielectric layers: polystyrene (PS) and poly (methyl methacrylate) (PMMA). The as-fabricated memory device exhibits multilevel non-volatile memory nature, as illustrated in Fig. 11. Figure 11a depicts the endurance of this NFGM, which is more than  $10^2$  times (under the condition of  $V_d = -5$  V and  $V_g = 0$  V). Programming process and corresponding voltages are shown in Fig. 11b, and the four voltage steps are from  $-80$  to  $80$  V ( $-80$ ,  $+30$ ,  $+50$ ,  $+80$  V). Figure 11c, d illustrates the retention characteristics by measuring four current levels ( $Abs(I_d)$  represents the absolute value of drain current) at  $V_d = -5$  V and  $V_g = 0$  V with 60 s delay, indicating the stable retention times after 10 years. This MoS<sub>2</sub>-based

organic FET is a 2-bit memory device controlled by  $V$  and potential for inexpensive memory devices.

## 6 Conclusions

In this paper, we have reviewed state-of-the-art approaches in MoS<sub>2</sub> FETs, such as progresses on manufacturing of MoS<sub>2</sub> FETs, MoS<sub>2</sub> FET-based memory devices, and MoS<sub>2</sub> FET-based sensors. To understanding the contact physics based on Schottky barrier, different species of metals utilized to achieve high-performance n-type and p-type MoS<sub>2</sub> FETs are reviewed, and optimization of ferromagnetic contact for spintronics applications are discussed too. Intrinsic properties measured by four-terminal measurements are highlighted, which is an effective method to estimate contact quality of MoS<sub>2</sub>-based FETs. In addition, gate dielectric formation and doping strategies are studied and provide guidelines for prospective manufacturing of MoS<sub>2</sub>-based FETs.

Low-frequency noise (LFN) analysis was carried out for studying the performance of MoS<sub>2</sub> FETs. FETs made of bilayer MoS<sub>2</sub> present a longer trap decay time. Further analysis shows that the LFN subjects not only to the physical properties of the channels but also the behavior of

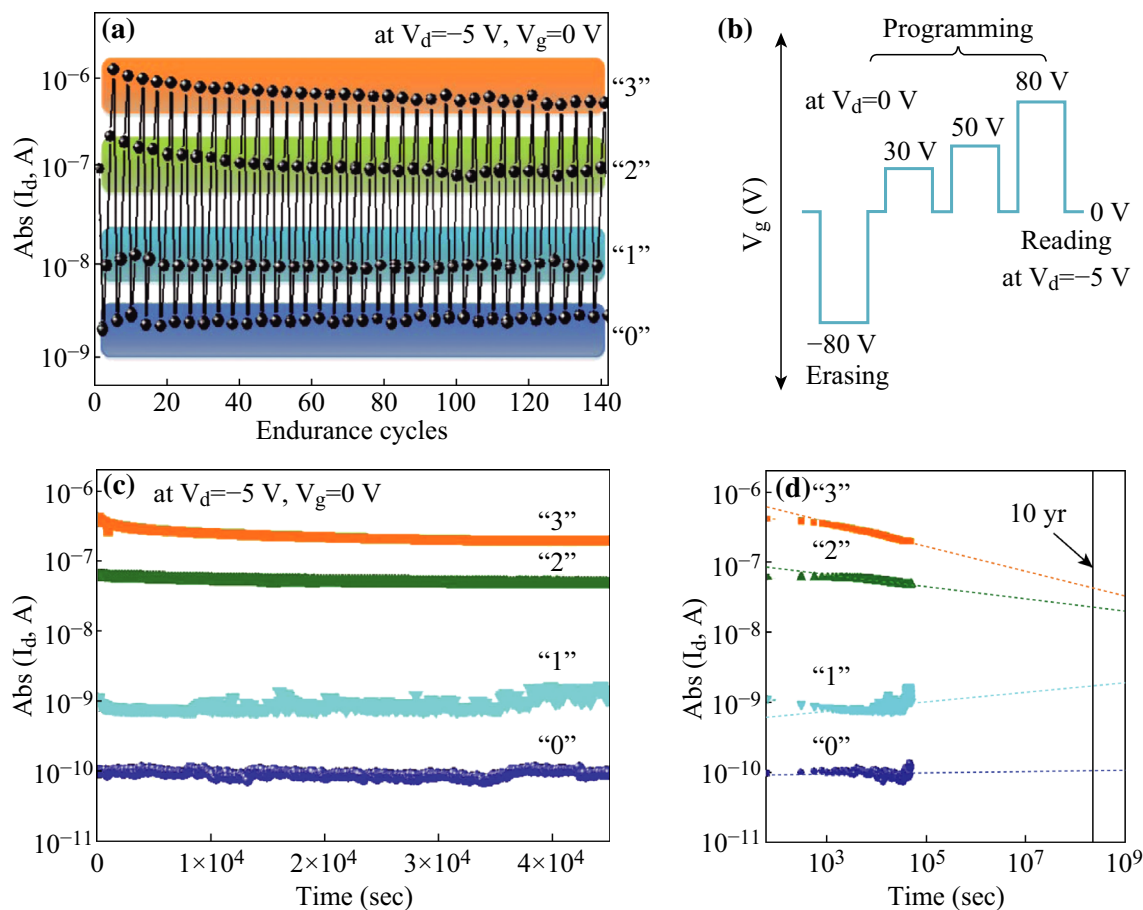


**Fig. 11** **a** Endurance measurement of as-fabricated NFGM under the condition of  $V_d = -5$  V and  $V_g = 0$  V. **b** Programming process and corresponding voltages are shown, four voltage steps are  $-80$ ,  $+30$ ,  $+50$ , and  $+80$  V. **c** and **d** illustrate the retention characteristics of four current levels at  $V_d = -5$  V and  $V_g = 0$  V with 60 s delay. Adopted from [98]

contacts in MoS<sub>2</sub> FETs. The noise increase in aged MoS<sub>2</sub> FETs is caused by aging of the MoS<sub>2</sub> channels rather than the aging of contacts. This phenomenon is significant in MoS<sub>2</sub> as well as in other 2D materials FETs for the optimization of channel implementation.

Photoresponse of MoS<sub>2</sub>-based FETs are critical and considered in this review, mainly focusing on the photocurrent generation with and without illumination. Moreover, MoS<sub>2</sub>-based FETs are utilized in gas and biological sensors, showing its high sensitivity and selectivity. MoS<sub>2</sub> nanoflakes are fabricated and successfully employed in organic nano-floating gate memories (NFGMs) as non-volatile random-access memory (NVRAM), providing an instance for nanomaterials used in memory devices. The plasma-treated MoS<sub>2</sub> FETs can serve as multibit memory devices and exhibit excellent storage capacities, suggesting the significance of plasma in performance improving of MoS<sub>2</sub> electronic devices.

To conclude, MoS<sub>2</sub> FETs based on thin-film and nano-size structures are investigated. Some key optical and electronic properties of these MoS<sub>2</sub> FET devices are unique

and superior than FETs made of conventional semiconductors, thus are suitable for novel electronic and optoelectronic applications.

**Open Access** This article is distributed under the terms of the Creative Commons Attribution License which permits any use, distribution, and reproduction in any medium, provided the original author(s) and the source are credited.

## References

1. D. Jariwala, V.K. Sangwan, L.J. Lauhon, T.J. Marks, M.C. Hersam, Emerging device applications for semiconducting two-dimensional transition metal dichalcogenides. *ACS Nano* **8**(2), 1102–1120 (2014). doi:10.1021/nn500064s
2. Q.H. Wang, K. Kalantar-Zadeh, A. Kis, J.N. Coleman, M.S. Strano, Electronics and optoelectronics of two-dimensional transition metal dichalcogenides. *Nat. Nanotechnol.* **7**(11), 699–712 (2012). doi:10.1038/nnano.2012.193
3. G. Plechinger, J. Mann, E. Preciado, D. Barroso, A. Nguyen, J. Eroms, C. Schueller, L. Bartels, T. Korn, A direct comparison of CVD-grown and exfoliated MoS<sub>2</sub> using optical spectroscopy. *Semicond. Sci Tech.* **29**(6), 064008 (2014). doi:10.1088/0268-1242/29/6/064008

4. E.S. Kadantsev, P. Hawrylak, Electronic structure of a single MoS<sub>2</sub> monolayer. *Solid State Commun.* **152**(10), 909–913 (2012). doi:[10.1016/j.ssc.2012.02.005](https://doi.org/10.1016/j.ssc.2012.02.005)
5. A. Kumar, P.K. Ahluwalia, A first principle comparative study of electronic and optical properties of 1H-MoS<sub>2</sub> and 2H-MoS<sub>2</sub>. *Mater. Chem. Phys.* **135**(2–3), 755–761 (2012). doi:[10.1016/j.matchemphys.2012.05.055](https://doi.org/10.1016/j.matchemphys.2012.05.055)
6. Q. Zhang, Y. Cheng, L.Y. Gan, U. Schwingenschloegl, Giant valley drifts in uniaxially strained monolayer MoS<sub>2</sub>. *Phys. Rev. B* **88**(24), 245447 (2013). doi:[10.1103/PhysRevB.88.245447](https://doi.org/10.1103/PhysRevB.88.245447)
7. B. Chakraborty, H.S.S.R. Matte, A.K. Sood, C.N.R. Rao, Layer-dependent resonant Raman scattering of a few layer MoS<sub>2</sub>. *J. Raman Spectrosc.* **44**(1), 92–96 (2013). doi:[10.1002/jrs.4147](https://doi.org/10.1002/jrs.4147)
8. Z.M. Wang, *MoS<sub>2</sub>: Materials, Physics, and Devices* (Springer, New York, 21, pp:1–291, 2014)
9. R. Frindt, Single crystals of MoS<sub>2</sub> several molecular layers thick. *J. Appl. Phys.* **37**(4), 1928–1929 (1966). doi:[10.1063/1.1708627](https://doi.org/10.1063/1.1708627)
10. Y.H. Lee, X.Q. Zhang, W. Zhang, M.T. Chang, C.T. Lin, K.D. Chang, Y.C. Yu, J.T.W. Wang, C.S. Chang, L.J. Li, T.W. Lin, Synthesis of large-area MoS<sub>2</sub> atomic layers with chemical vapor deposition. *Adv. Mater.* **24**(17), 2320–2325 (2012). doi:[10.1002/adma.201104798](https://doi.org/10.1002/adma.201104798)
11. H. Pan, Y.W. Zhang, Tuning the electronic and magnetic properties of MoS<sub>2</sub> nanoribbons by strain engineering. *J. Phys. Chem. C* **116**(21), 11752–11757 (2012). doi:[10.1021/jp3015782](https://doi.org/10.1021/jp3015782)
12. Z. Zhou, Y. Lin, P. Zhang, E. Ashalley, M. Shafa, H. Li, J. Wu, Z. Wang, Hydrothermal fabrication of porous MoS<sub>2</sub> and its visible light photocatalytic properties. *Mater. Lett.* **131**, 122–124 (2014). doi:[10.1016/j.matlet.2014.05.162](https://doi.org/10.1016/j.matlet.2014.05.162)
13. R. van Leeuwen, A. Castellanos-Gomez, G.A. Steele, H.S.J. van der Zant, W.J. Venstra, Time-domain response of atomically thin MoS<sub>2</sub> nanomechanical resonators. *Appl. Phys. Lett.* **105**(4), 041911 (2014). doi:[10.1063/1.4892072](https://doi.org/10.1063/1.4892072)
14. Z. Yin, H. Li, H. Li, L. Jiang, Y. Shi, Y. Sun, G. Lu, Q. Zhang, X. Chen, H. Zhang, Single-layer MoS<sub>2</sub> phototransistors. *ACS Nano* **6**(1), 74–80 (2012). doi:[10.1021/nl2024557](https://doi.org/10.1021/nl2024557)
15. F.K. Perkins, A.L. Friedman, E. Cobas, P.M. Campbell, G.G. Jernigan, B.T. Jonker, Chemical vapor sensing with monolayer MoS<sub>2</sub>. *Nano Lett.* **13**(2), 668–673 (2013). doi:[10.1021/nl3043079](https://doi.org/10.1021/nl3043079)
16. O. Lopez-Sanchez, D. Lembke, M. Kayci, A. Radenovic, A. Kis, Ultrasensitive photodetectors based on monolayer MoS<sub>2</sub>. *Nat. Nanotechnol.* **8**(7), 497–501 (2013). doi:[10.1038/nnano.2013.100](https://doi.org/10.1038/nnano.2013.100)
17. B. Radisavljevic, M.B. Whitwick, A. Kis, Small-signal amplifier based on single-layer MoS<sub>2</sub>. *Appl. Phys. Lett.* **101**(4), 043103 (2012). doi:[10.1063/1.4738986](https://doi.org/10.1063/1.4738986)
18. S. Ding, D. Zhang, J.S. Chen, X.W. Lou, Facile synthesis of hierarchical MoS<sub>2</sub> microspheres composed of few-layered nanosheets and their lithium storage properties. *Nanoscale* **4**(1), 95–98 (2012). doi:[10.1039/c1nr11552a](https://doi.org/10.1039/c1nr11552a)
19. K. Chang, W. Chen, L-cysteine-assisted synthesis of layered MoS<sub>2</sub>/graphene composites with excellent electrochemical performances for lithium ion batteries. *ACS Nano* **5**(6), 4720–4728 (2011). doi:[10.1021/nl200659w](https://doi.org/10.1021/nl200659w)
20. K.F. Mak, K. He, J. Shan, T.F. Heinz, Control of valley polarization in monolayer MoS<sub>2</sub> by optical helicity. *Nat. Nanotechnol.* **7**(8), 494–498 (2012). doi:[10.1038/nnano.2012.96](https://doi.org/10.1038/nnano.2012.96)
21. H. Zeng, J. Dai, W. Yao, D. Xiao, X. Cui, Valley polarization in MoS<sub>2</sub> monolayers by optical pumping. *Nat. Nanotechnol.* **7**(8), 490–493 (2012). doi:[10.1038/nnano.2012.95](https://doi.org/10.1038/nnano.2012.95)
22. X. Huang, Z. Yin, S. Wu, X. Qi, Q. He, Q. Zhang, Q. Yan, F. Boey, H. Zhang, Graphene-based materials: synthesis, characterization, properties, and applications. *Small* **7**(14), 1876–1902 (2011). doi:[10.1002/sml.201002009](https://doi.org/10.1002/sml.201002009)
23. H.S. Lee, S.W. Min, Y.G. Chang, M.K. Park, T. Nam, H. Kim, J.H. Kim, S. Ryu, S. Im, MoS<sub>2</sub> nanosheet phototransistors with thickness-modulated optical energy gap. *Nano Lett.* **12**(7), 3695–3700 (2012). doi:[10.1021/nl301485q](https://doi.org/10.1021/nl301485q)
24. H. Liu, J.J. Gu, P.D. Ye, MoS<sub>2</sub> nanoribbon transistors: transition from depletion mode to enhancement mode by channel-width trimming. *IEEE Electr. Device L* **33**(9), 1273–1275 (2012). doi:[10.1109/LED.2012.2202630](https://doi.org/10.1109/LED.2012.2202630)
25. X. Wang, S. Yang, Q. Yue, F. Wu, J. Li, Response of MoS<sub>2</sub> nanosheet field effect transistor under different gas environments and its long wavelength photoresponse characteristics. *J. Alloy. Compd.* **615**, 989–993 (2014). doi:[10.1016/j.jallcom.2014.07.016](https://doi.org/10.1016/j.jallcom.2014.07.016)
26. G. Eda, H. Yamaguchi, D. Voiry, T. Fujita, M. Chen, M. Chhowalla, Photoluminescence from chemically exfoliated MoS<sub>2</sub>. *Nano Lett.* **11**(12), 5111–5116 (2011). doi:[10.1021/nl201874w](https://doi.org/10.1021/nl201874w)
27. B. Radisavljevic, A. Radenovic, J. Brivio, V. Giacometti, A. Kis, Single-layer MoS<sub>2</sub> transistors. *Nat. Nanotechnol.* **6**(3), 147–150 (2011). doi:[10.1038/nnano.2010.279](https://doi.org/10.1038/nnano.2010.279)
28. Y. Yoon, K. Ganapathi, S. Salahuddin, How good can monolayer MoS<sub>2</sub> transistors be? *Nano Lett.* **11**(9), 3768–3773 (2011). doi:[10.1021/nl2018178](https://doi.org/10.1021/nl2018178)
29. F. Leonard, A.A. Talin, Electrical contacts to one- and two-dimensional nanomaterials. *Nat. Nanotechnol.* **6**(12), 773–783 (2011). doi:[10.1038/nnano.2011.196](https://doi.org/10.1038/nnano.2011.196)
30. Y. Du, L. Yang, H. Liu, P.D. Ye, Contact research strategy for emerging molybdenum disulfide and other two-dimensional field-effect transistors. *Appl. Mater.* **2**(9), 092510 (2014). doi:[10.1063/1.4894198](https://doi.org/10.1063/1.4894198)
31. H. Liu, A.T. Neal, P.D. Ye, Channel length scaling of MoS<sub>2</sub> MOS-FETs. *ACS Nano* **6**(10), 8563–8569 (2012). doi:[10.1021/nl303513c](https://doi.org/10.1021/nl303513c)
32. S. Das, H.Y. Chen, A.V. Penumatcha, J. Appenzeller, High performance multilayer MoS<sub>2</sub> transistors with scandium contacts. *Nano Lett.* **13**(1), 100–105 (2013). doi:[10.1021/nl303583v](https://doi.org/10.1021/nl303583v)
33. J.H. Kang, D. Sarkar, W. Liu, D. Jena, K. Banerjee, A computational study of metal-contacts to beyond-graphene 2D semiconductor materials. 2012 IEEE Int. Electr. Devices Meet. (IEDM) (2012). doi:[10.1109/IEDM.2012.6479060](https://doi.org/10.1109/IEDM.2012.6479060)
34. W. Liu, J.H. Kang, W. Cao, D. Sarkar, Y. Khatami, D. Jena, K. Banerjee, High-performance few-layer-MoS<sub>2</sub> field-effect-transistor with record low contact-resistance, 2013 IEEE Int. Electr. Devices Meet. (IEDM) (2013). doi:[10.1109/IEDM.2013.6724660](https://doi.org/10.1109/IEDM.2013.6724660)
35. J. Kang, W. Liu, K. Banerjee, High-performance MoS<sub>2</sub> transistors with low-resistance molybdenum contacts. *Appl. Phys. Lett.* **104**(9), 093106 (2014). doi:[10.1063/1.4866340](https://doi.org/10.1063/1.4866340)
36. S. Kim, A. Konar, W.S. Hwang, J.H. Lee, J. Lee, J. Yang, C. Jung, H. Kim, J.B. Yoo, J.Y. Choi, Y.W. Jin, S.Y. Lee, D. Jena, W. Choi, K. Kim, High-mobility and low-power thin-film transistors based on multilayer MoS<sub>2</sub> crystals. *Nat. Commun.* **3**, 1011 (2012). doi:[10.1038/ncomms2018](https://doi.org/10.1038/ncomms2018)
37. M. Fontana, T. Deppe, A.K. Boyd, M. Rinzan, A.Y. Liu, M. Paranjape, P. Barbara, Electron-hole transport and photovoltaic effect in gated MoS<sub>2</sub> Schottky junctions. *Sci. Rep-UK* **3**, 1634 (2013). doi:[10.1038/srep01634](https://doi.org/10.1038/srep01634)
38. S. Chuang, C. Battaglia, A. Azcatl, S. McDonnell, J.S. Kang, X. Yin, M. Tosun, R. Kapadia, H. Fang, R.M. Wallace, A. Javey, MoS<sub>2</sub> p-type transistors and diodes enabled by high work function mxx contacts. *Nano Lett.* **14**(3), 1337–1342 (2014). doi:[10.1021/nl40043505](https://doi.org/10.1021/nl40043505)
39. C. Battaglia, X. Yin, M. Zheng, I.D. Sharp, T. Chen, S. McDonnell, A. Azcatl, C. Carraro, B. Ma, R. Maboudian, R.M. Wallace, A. Javey, Hole selective MoO<sub>x</sub> contact for silicon solar cells. *Nano Lett.* **14**(2), 967–971 (2014). doi:[10.1021/nl404389u](https://doi.org/10.1021/nl404389u)
40. I. Popov, G. Seifert, D. Tomanek, Designing electrical contacts to MoS<sub>2</sub> monolayers: a computational study. *Phys. Rev. Lett.* **108**(15), 156802 (2012). doi:[10.1103/PhysRevLett.108.156802](https://doi.org/10.1103/PhysRevLett.108.156802)
41. J.-R. Chen, P.M. Odenthal, A.G. Swartz, G.C. Floyd, H. Wen, K.Y. Luo, R.K. Kawakami, Control of schottky barriers in single

- layer MoS<sub>2</sub> transistors with ferromagnetic contacts. *Nano Lett.* **13**(7), 3106–3110 (2013). doi:[10.1021/nl4010157](https://doi.org/10.1021/nl4010157)
42. A. Dankert, L. Langouche, M.V. Kamalakar, S.P. Dash, High-performance molybdenum disulfide field-effect transistors with spin tunnel contacts. *ACS Nano* **8**(1), 476–482 (2014). doi:[10.1021/nn404961e](https://doi.org/10.1021/nn404961e)
  43. N.R. Pradhan, D. Rhodes, Q. Zhang, S. Talapatra, M. Terrones, P.M. Ajayan, L. Balicas, Intrinsic carrier mobility of multi-layered MoS<sub>2</sub> field-effect transistors on SiO<sub>2</sub>. *Appl. Phys. Lett.* **102**(12), 123105 (2013). doi:[10.1063/1.4799172](https://doi.org/10.1063/1.4799172)
  44. W. Bao, X. Cai, D. Kim, K. Sridhara, M.S. Fuhrer, High mobility ambipolar MoS<sub>2</sub> field-effect transistors: substrate and dielectric effects. *Appl. Phys. Lett.* **102**(4), 042104 (2013). doi:[10.1063/1.4789365](https://doi.org/10.1063/1.4789365)
  45. B.W.H. Baugher, H.O.H. Churchill, Y. Yang, P. Jarillo-Herrero, Intrinsic electronic transport properties of high-quality monolayer and bilayer MoS<sub>2</sub>. *Nano Lett.* **13**(9), 4212–4216 (2013). doi:[10.1021/nl401916s](https://doi.org/10.1021/nl401916s)
  46. N.R. Pradhan, D. Rhodes, Y. Xin, S. Memaran, L. Bhaskaran, M. Siddiq, S. Hill, P.M. Ajayan, L. Balicas, Ambipolar molybdenum diselenide field-effect transistors: field-effect and hall mobilities. *ACS Nano* **8**(8), 7923–7929 (2014). doi:[10.1021/nn501693d](https://doi.org/10.1021/nn501693d)
  47. J. Yoon, W. Park, G.Y. Bae, Y. Kim, H.S. Jang, Y. Hyun, S.K. Lim, Y.H. Kahng, W.K. Hong, B.H. Lee, H.C. Ko, Highly flexible and transparent multilayer MoS<sub>2</sub> transistors with graphene electrodes. *Small* **9**(19), 3295–3300 (2013). doi:[10.1002/sml.201300134](https://doi.org/10.1002/sml.201300134)
  48. R. Kappera, D. Voiry, S.E. Yalcin, B. Branch, G. Gupta, A.D. Mohite, M. Chhowalla, Phase-engineered low-resistance contacts for ultrathin MoS<sub>2</sub> transistors. *Nat. Mater.* **13**(12), 1128–1134 (2014). doi:[10.1038/nmat4080](https://doi.org/10.1038/nmat4080)
  49. M. Amani, M.L. Chin, A.G. Birdwell, T.P. O'Regan, S. Najmaei, Z. Liu, P.M. Ajayan, J. Lou, M. Dubey, Electrical performance of monolayer MoS<sub>2</sub> field-effect transistors prepared by chemical vapor deposition. *Appl. Phys. Lett.* **102**(19), 193107 (2013). doi:[10.1063/1.4804546](https://doi.org/10.1063/1.4804546)
  50. H. Wang, L. Yu, Y.H. Lee, Y. Shi, A. Hsu, M.L. Chin, L.-J. Li, M. Dubey, J. Kong, T. Palacios, Integrated circuits based on bilayer MoS<sub>2</sub> transistors. *Nano Lett.* **12**(9), 4674–4680 (2012). doi:[10.1021/nl302015v](https://doi.org/10.1021/nl302015v)
  51. L. Zeng, Z. Xin, S. Chen, G. Du, J. Kang, X. Liu, Remote phonon and impurity screening effect of substrate and gate dielectric on electron dynamics in single layer MoS<sub>2</sub>. *Appl. Phys. Lett.* **103**(11), 113505 (2013). doi:[10.1063/1.4821344](https://doi.org/10.1063/1.4821344)
  52. D. Jena, A. Konar, Enhancement of carrier mobility in semiconductor nanostructures by dielectric engineering. *Phys. Rev. Lett.* **98**(13), 136805 (2007). doi:[10.1103/PhysRevLett.98.136805](https://doi.org/10.1103/PhysRevLett.98.136805)
  53. H. Liu, K. Xu, X. Zhang, P.D. Ye, The integration of high-*k* dielectric on two-dimensional crystals by atomic layer deposition. *Appl. Phys. Lett.* **100**(15), 152115 (2012). doi:[10.1063/1.3703595](https://doi.org/10.1063/1.3703595)
  54. J. Swerts, N. Peys, L. Nyns, A. Delabie, A. Franquet, J.W. Maes, S. Van Elshocht, S. De Gendt, Impact of precursor chemistry and process conditions on the scalability of ALD HfO<sub>2</sub> gate dielectrics. *J. Electrochem. Soc.* **157**(1), G26–G31 (2010). doi:[10.1149/1.3258664](https://doi.org/10.1149/1.3258664)
  55. J. Yang, S. Kim, W. Choi, S.H. Park, Y. Jung, M.H. Cho, H. Kim, Improved growth behavior of atomic-layer-deposited high-*k* dielectrics on multilayer MoS<sub>2</sub> by oxygen plasma pretreatment. *ACS Appl. Mater. Inter.* **5**(11), 4739–4744 (2013). doi:[10.1021/am303261c](https://doi.org/10.1021/am303261c)
  56. A. Azcatl, S. McDonnell, K.C. Santosh, X. Peng, H. Dong, X. Qin, R. Addou, G.I. Mordi, N. Lu, J. Kim, M.J. Kim, K. Cho, R.M. Wallace, MoS<sub>2</sub> functionalization for ultra-thin atomic layer deposited dielectrics. *Appl. Phys. Lett.* **104**(11), 111601 (2014). doi:[10.1063/1.4869149](https://doi.org/10.1063/1.4869149)
  57. L. Cheng, X. Qin, A.T. Lucero, A. Azcatl, J. Huang, R.M. Wallace, K. Cho, J. Kim, Atomic layer deposition of a high-*k* dielectric on MoS<sub>2</sub> using trimethylaluminum and ozone. *ACS Appl. Mater. Inter.* **6**(15), 11834–11838 (2014). doi:[10.1021/am5032105](https://doi.org/10.1021/am5032105)
  58. Y. Du, H. Liu, A.T. Neal, M. Si, P.D. Ye, Molecular doping of multilayer MoS<sub>2</sub> field-effect transistors: reduction in sheet and contact resistances. *IEEE Electr. Device L.* **34**(10), 1328–1330 (2013). doi:[10.1109/LED.2013.2277311](https://doi.org/10.1109/LED.2013.2277311)
  59. J.D. Lin, C. Han, F. Wang, R. Wang, D. Xiang, S. Qin, X.A. Zhang, L. Wang, H. Zhang, A.T.S. Wee, W. Chen, Electron-doping-enhanced trion formation in monolayer molybdenum disulfide functionalized with cesium carbonate. *ACS Nano* **8**(5), 5323–5329 (2014). doi:[10.1021/nn501580c](https://doi.org/10.1021/nn501580c)
  60. H. Fang, M. Tosun, G. Seol, T.C. Chang, K. Takei, J. Guo, A. Javey, Degenerate n-doping of few-layer transition metal dichalcogenides by potassium. *Nano Lett.* **13**(5), 1991–1995 (2013). doi:[10.1021/nl400044m](https://doi.org/10.1021/nl400044m)
  61. D. Kiriya, M. Tosun, P. Zhao, J.S. Kang, A. Javey, Air-stable surface charge transfer doping of MoS<sub>2</sub> by benzyl viologen. *JACS* **136**(22), 7853–7856 (2014). doi:[10.1021/ja5033327](https://doi.org/10.1021/ja5033327)
  62. L. Yang, K. Majumdar, H. Liu, Y. Du, H. Wu, M. Hatzistergos, P.Y. Hung, R. Tieckelmann, W. Tsai, C. Hobbs, P.D. Ye, Chloride molecular doping technique on 2D materials: WS<sub>2</sub> and MoS<sub>2</sub>. *Nano Lett.* **14**(11), 6275–6280 (2014). doi:[10.1021/nl502603d](https://doi.org/10.1021/nl502603d)
  63. Y. Wu, Y. Lin, A.A. Bol, K.A. Jenkins, F. Xia, D.B. Farmer, Y. Zhu, P. Avouris, High-frequency, scaled graphene transistors on diamond-like carbon. *Nature* **472**(7341), 74–78 (2011). doi:[10.1038/nature09979](https://doi.org/10.1038/nature09979)
  64. J.B. Johnson, The Schottky effect in low frequency circuits. *Phys. Rev.* **26**(1), 71 (1925). doi:[10.1103/PhysRev.26.71](https://doi.org/10.1103/PhysRev.26.71)
  65. B.H. Calhoun, A. Wang, A. Chandrakasan, Device sizing for minimum energy operation in subthreshold circuits. (pp: 95–98, 3–6 Oct. 2004). doi:[10.1109/CICC.2004.1358745](https://doi.org/10.1109/CICC.2004.1358745)
  66. J.M. Chang, A.A. Abidi, C.R. Viswanathan, Flicker noise in CMOS transistors from subthreshold to strong inversion at various temperatures. *IEEE Trans. Electron Devices* **41**(11), 1965–1971 (1994). doi:[10.1109/16.333812](https://doi.org/10.1109/16.333812)
  67. S. Ghatak, A.N. Pal, A. Ghosh, Nature of electronic states in atomically thin MoS<sub>2</sub> field-effect transistors. *ACS Nano* **5**(10), 7707–7712 (2011). doi:[10.1021/nn202852j](https://doi.org/10.1021/nn202852j)
  68. B. Radisavljevic, M.B. Whitwick, A. Kis, Integrated circuits and logic operations based on single-layer MoS<sub>2</sub>. *ACS Nano* **5**(12), 9934–9938 (2011). doi:[10.1021/nn203715c](https://doi.org/10.1021/nn203715c)
  69. C. Kayis, J.H. Leach, C.Y. Zhu, M. Wu, X. Li, U. Oezguer, H. Morkoc, X. Yang, V. Misra, P.H. Handel, Low-frequency noise measurements of AlGaIn/GaN metal-oxide-semiconductor heterostructure field-effect transistors with HfAlO gate dielectric. *IEEE Electr. Device L.* **31**(9), 1041–1043 (2010). doi:[10.1109/LED.2010.2055823](https://doi.org/10.1109/LED.2010.2055823)
  70. A.A. Balandin, *Noise and Fluctuations Control in Electronic Devices* (American Scientific Publishers, Los Angeles, pp.1–411, 2002)
  71. E. Simoen, A. Mercha, C. Claeys, E. Young, Correlation between the 1/f noise parameters and the effective low-field mobility in HfO<sub>2</sub> gate dielectric n-channel metal-oxide-semiconductor field-effect transistors. *Appl. Phys. Lett.* **85**(6), 1057–1059 (2004). doi:[10.1063/1.1779967](https://doi.org/10.1063/1.1779967)
  72. X. Xie, D. Sarkar, W. Liu, J. Kang, O. Marinov, M.J. Deen, K. Banerjee, Low-frequency noise in bilayer MoS<sub>2</sub> transistor. *ACS Nano* **8**(6), 5633–5640 (2014). doi:[10.1021/nn4066473](https://doi.org/10.1021/nn4066473)
  73. V.K. Sangwan, H.N. Arnold, D. Jariwala, T.J. Marks, L.J. Lauhon, M.C. Hersam, Low-frequency electronic noise in single-layer MoS<sub>2</sub> transistors. *Nano Lett.* **13**(9), 4351–4355 (2013). doi:[10.1021/nl402150r](https://doi.org/10.1021/nl402150r)

74. H.-J. Kwon, H. Kang, J. Jang, S. Kim, C.P. Grigoropoulos, Analysis of flicker noise in two-dimensional multilayer MoS<sub>2</sub> transistors. *Appl. Phys. Lett.* **104**(8), 083110 (2014). doi:[10.1063/1.4866785](https://doi.org/10.1063/1.4866785)
75. J. Renteria, R. Samnakay, S.L. Rumyantsev, C. Jiang, P. Goli, M.S. Shur, A.A. Balandin, Low-frequency 1/f noise in MoS<sub>2</sub> transistors: relative contributions of the channel and contacts. *Appl. Phys. Lett.* **104**(15), 153104 (2014). doi:[10.1063/1.4871374](https://doi.org/10.1063/1.4871374)
76. S. Ghatak, S. Mukherjee, M. Jain, D.D. Sarma, A. Ghosh, Microscopic origin of low frequency noise in MoS<sub>2</sub> field-effect transistors. *Appl. Mater.* **2**(9), 092515 (2014). doi:[10.1063/1.4895955](https://doi.org/10.1063/1.4895955)
77. A.M. Jones, H. Yu, N.J. Ghimire, S. Wu, G. Aivazian, J.S. Ross, B. Zhao, J. Yan, D.G. Mandrus, D. Xiao, W. Yao, X. Xu, Optical generation of excitonic valley coherence in monolayer WSe<sub>2</sub>. *Nat. Nanotechnol.* **8**(9), 634–638 (2013). doi:[10.1038/nnano.2013.151](https://doi.org/10.1038/nnano.2013.151)
78. N.R. Pradhan, S. Memaran, D.R.Z. Lu, J. Ludwig, Q. Zhou, P. Ajayan, D. Smirnov, L. Balicas, Pronounced photovoltaic response from PN-junctions of multi-layered MoSe<sub>2</sub> on h-BN. *arXiv:1411.2086* (2014)
79. H.M. Li, D.Y. Lee, M.S. Choi, D. Qu, X. Liu, C.H. Ra, W.J. Yoo, Metal-semiconductor barrier modulation for high photoresponse in transition metal dichalcogenide field effect transistors. *SCI Rep-UK* **4**, 4041 (2014). doi:[10.1038/srep04041](https://doi.org/10.1038/srep04041)
80. M.F. Khan, M.W. Iqbal, M.Z. Iqbal, M.A. Shehzad, Y. Seo, J. Eom, Photocurrent response of MoS<sub>2</sub> field-effect transistor by deep ultraviolet light in atmospheric and N<sub>2</sub> gas environments. *ACS Appl. Mater. Interface* **6**(23), 21645–21651 (2014). doi:[10.1021/am506716a](https://doi.org/10.1021/am506716a)
81. K. Cho, T.Y. Kim, W. Park, J. Park, D. Kim, J. Jang, H. Jeong, S. Hong, T. Lee, Gate-bias stress-dependent photoconductive characteristics of multi-layer MoS<sub>2</sub> field-effect transistors. *Nanotechnology* **25**(15), 155201 (2014). doi:[10.1088/0957-4484/25/15/155201](https://doi.org/10.1088/0957-4484/25/15/155201)
82. D.S. Tsai, D.H. Lien, M.L. Tsai, S.H. Su, K.M. Chen, J.J. Ke, Y.C. Yu, L.J. Li, J.H. He, Trilayered MoS<sub>2</sub> metal-semiconductor-metal photodetectors: photogain and radiation resistance. *IEEE J. Sel. Top. Quantum* **20**(1), 3800206 (2014). doi:[10.1109/JSTQE.2013.2268383](https://doi.org/10.1109/JSTQE.2013.2268383)
83. A. Sobhani, A. Lauchner, S. Najmaei, C. Ayala-Orozco, F. Wen, J. Lou, N.J. Halas, Enhancing the photocurrent and photoluminescence of single crystal monolayer MoS<sub>2</sub> with resonant plasmonic nanoshells. *Appl. Phys. Lett.* **104**(3), 031112 (2014). doi:[10.1063/1.4862745](https://doi.org/10.1063/1.4862745)
84. X. Hong, J. Kim, S.F. Shi, Y. Zhang, C. Jin, Y. Sun, S. Tongay, J. Wu, Y. Zhang, F. Wang, Ultrafast charge transfer in atomically thin MoS<sub>2</sub>/WS<sub>2</sub> heterostructures. *Nat. Nanotechnol.* **9**(9), 682–686 (2014). doi:[10.1038/nnano.2014.167](https://doi.org/10.1038/nnano.2014.167)
85. N. Huo, J. Kang, Z. Wei, S.S. Li, J. Li, S.H. Wei, Novel and enhanced optoelectronic performances of multilayer MoS<sub>2</sub>-WS<sub>2</sub> heterostructure transistors. *Adv. Funct. Mater.* **24**(44), 7025–7031 (2014). doi:[10.1002/adfm.201401504](https://doi.org/10.1002/adfm.201401504)
86. D. Sarkar, W. Liu, X. Xie, A.C. Anselmo, S. Mitragotri, K. Banerjee, MoS<sub>2</sub> field-effect transistor for next-generation label-free biosensors. *ACS Nano* **8**(4), 3992–4003 (2014). doi:[10.1021/nm5009148](https://doi.org/10.1021/nm5009148)
87. L. Wang, Y. Wang, J.I. Wong, T. Palacios, J. Kong, H.Y. Yang, Functionalized MoS<sub>2</sub> nanosheet-based field-effect biosensor for label-free sensitive detection of cancer marker proteins in solution. *Small* **10**(6), 1101–1105 (2014). doi:[10.1002/sml.201302081](https://doi.org/10.1002/sml.201302081)
88. B. Liu, L. Chen, G. Liu, A.N. Abbas, M. Fathi, C. Zhou, High-performance chemical sensing using Schottky-contacted chemical vapor deposition grown mono layer MoS<sub>2</sub> transistors. *ACS Nano* **8**(5), 5304–5314 (2014). doi:[10.1021/nn5015215](https://doi.org/10.1021/nn5015215)
89. S. Najmaei, Z. Liu, W. Zhou, X. Zou, G. Shi, S. Lei, B.I. Yakobson, J.C. Idrobo, P.M. Ajayan, J. Lou, Vapour phase growth and grain boundary structure of molybdenum disulphide atomic layers. *Nat. Mater.* **12**(8), 754–759 (2013). doi:[10.1038/nmat3673](https://doi.org/10.1038/nmat3673)
90. H. Li, Z. Yin, Q. He, H. Li, X. Huang, G. Lu, D.W.H. Fam, A.I.Y. Tok, Q. Zhang, H. Zhang, Fabrication of single-and multilayer MoS<sub>2</sub> film-based field-effect transistors for sensing NO at room temperature. *Small* **8**(1), 63–67 (2012). doi:[10.1002/sml.201101016](https://doi.org/10.1002/sml.201101016)
91. D.J. Late, Y.K. Huang, B. Liu, J. Acharya, S.N. Shirodkar, J. Luo, A. Yan, D. Charles, U.V. Waghmare, V.P. Dravid, C.N.R. Rao, Sensing behavior of atomically thin-layered MoS<sub>2</sub> transistors. *ACS Nano* **7**(6), 4879–4891 (2013). doi:[10.1021/nn400026u](https://doi.org/10.1021/nn400026u)
92. A.L. Friedman, F.K. Perkins, E. Cobas, G.G. Jernigan, P.M. Campbell, A.T. Hanbicki, B.T. Jonker, Chemical vapor sensing of two-dimensional MoS<sub>2</sub> field effect transistor devices. *Solid State Electron.* **101**, 2–7 (2014). doi:[10.1016/j.sse.2014.06.013](https://doi.org/10.1016/j.sse.2014.06.013)
93. J. Lee, P. Dak, Y. Lee, H. Park, W. Choi, M.A. Alam, S. Kim, Two-dimensional layered MoS<sub>2</sub> biosensors enable highly sensitive detection of biomolecules. *Sci. Rep.* **4**, 7352 (2014). doi:[10.1038/srep07352](https://doi.org/10.1038/srep07352)
94. Y. Guo, C. Di, S. Ye, X. Sun, J. Zheng, Y. Wen, W. Wu, G. Yu, Y. Liu, Multibit storage of organic thin-film field-effect transistors. *Adv. Mater.* **21**(19), 1954–1959 (2009). doi:[10.1002/adma.200802430](https://doi.org/10.1002/adma.200802430)
95. J.I. Sohn, S.S. Choi, S.M. Morris, J.S. Bendall, H.J. Coles, W.K. Hong, G. Jo, T. Lee, M.E. Welland, Novel nonvolatile memory with multibit storage based on a ZnO nanowire transistor. *Nano Lett.* **10**(11), 4316–4320 (2010). doi:[10.1021/nl1013713](https://doi.org/10.1021/nl1013713)
96. T. Nirschl, J.B. Philipp, T.D. Flapp, G.W. Burr, B. Rajendran, M.H. Leao, A. Schrott, M. Yang, M. Breitwisch, C.F. Chen, E. Joseph, M. Lamorey, R. Cheek, S.H. Chen, S. Zaidi, S. Raoux, Y.C. Chen, Y. Zhu, R. Bergmann, H.L. Lung, C. Lam, Write strategies for 2 and 4-bit multi-level phase-change memory. *IEEE Electr. Devices Meet.* (pp: 461–464, 10–12 Dec. 2007). doi:[10.1109/IEDM.2007.4418973](https://doi.org/10.1109/IEDM.2007.4418973)
97. M. Chen, H. Nam, S. Wi, G. Priessnitz, I.M. Gunawan, X. Liang, Multibit data storage states formed in plasma-treated MoS<sub>2</sub> transistors. *ACS Nano* **8**(4), 4023–4032 (2014). doi:[10.1021/nm501181t](https://doi.org/10.1021/nm501181t)
98. M. Kang, Y.A. Kim, J.M. Yun, D. Khim, J. Kim, Y.Y. Noh, K.J. Baeg, D.Y. Kim, Stable charge storing in two-dimensional MoS<sub>2</sub> nanoflake floating gates for multilevel organic flash memory. *Nanoscale* **6**(21), 12315–12323 (2014). doi:[10.1039/C4NR03448A](https://doi.org/10.1039/C4NR03448A)